THESIS REPORT
Master's Degree

SYSTEMS
RESEARCH
CENTER

Supported by the National Science Foundation Engineering Research Center Program (NSFD CD 8803012), the University of Maryland, Harvard University, and Industry

Impact and Force Control of Flexible Manipulators

by I. Salmatjidis
Advisor: P.S. Krishnaprasad

M.S. 91-5

ABSTRACT

Title of Thesis: IMPACT AND FORCE CONTROL OF FLEXIBLE MANIPULATORS

Name of degree candidate: Ioanis Salmatjidis

Degree and Year: Master of Science, 1991

Thesis directed by: P. S. Krishnaprasad
Professor
Electrical Engineering

We consider the force control problem of a one degree-of-freedom flexible robot manipulator. We approximate the distributed parameter flexible structure by a finite number of rigid elements connected by means of torsional springs. We assume that the arm tip interacts with the environment under rigid, frictionless, point contact conditions. The kinematic (holonomic) constraints which hold when contact is established, are derived using the geometry of the problem. The free and constrained motion of the arm are predicted numerically using the Newmark integration method. Numerical results are compared to the

empirical system response. The conventional energy principle method for predicting the maximum reaction force is demonstrated, along with a much more efficient method based on the evaluation of instantaneous velocity increments just after impact. The latter assumes that velocities vary linearly between the time instants of initial contact and maximum force occurrence. Finally, a hybrid impact-force real-time controller for diminishing the impact effect is implemented and various design considerations are presented.

IMPACT AND FORCE CONTROL OF FLEXIBLE MANIPULATORS

by

Ioanis Salmatjidis

Thesis submitted to the Faculty of the Graduate School
of The University of Maryland in partial fulfillment
of the requirements for the degree of
Master of Science
1991

Advisory Committee:

Professor P. S. Krishnaprasad, Chairman/Advisor
Assistant Research Scientist Josip Lončarić/Coadvisor
Associate Professor Mark Austin

DEDICATION

To my parents Dimitris and Lephkothea

ACKNOWLEDGEMENTS

I am indebted to both my research advisors, Dr. P.S. Krishnaprasad and Dr. Lončarić, for their continuous support, encouragement and contribution throughout the course of this work. I am especially thankful to Dr. Krishnaprasad for his extensive tutoring, which greatly helped develop my understanding of the subject.

I would like to thank Dr. Mark Austin for serving as a member of my thesis advisory committee, my colleague Mark Desilets for his programming assistance and Dimitris Tsakiris for the many helpful discussions.

Also, I would like to express my gratitude to the Fulbright Foundation which partially covered my expenses during the first year of my graduate studies.

This research was supported in part by the National Science Foundation's Engineering Research Centers Program: NSFD CDR8803012 and by the AFOSR University Research Initiative Program under grant AFOSR-90-0105.

Contents

List of Tables

List of Figures

Chapter 1

Introduction

Research work in impact dynamics as it pertains to robotics appears to be scant in comparison to work on force and trajectory control of robot manipulators. In the context of trajectory control, the manipulator moves in a free space without any interaction with the environment. In force control a manipulator interacts with the environment while the controller attempts to maintain a force trajectory. Such applications include assembly lines, polishing etc. In the transition between the no-interaction and interaction modes, impact occurs. During the impact phenomena, which last only short periods of time, energy transfer takes place. Generally, high forces appear at the point or points of contact and at the joints of the manipulator as well, which could be harmful to the robot or the workpiece.

As far as controller design is concerned, there are three modes of operation so that a robot completes a task: motion in free space, impact and constrained

motion. For different tasks the strategy for the task to be completed might be different. Therefore, the controller should decide what kinds of operations are needed for each mode and when to change from one modé to another. In each mode, different kinds of feedback information might be used. For example, in the unconstrained subspace of the state space, it is the position of the end-effector to be specified and controlled, while in the constrained subspace it is the torque or force feedback that determine the control actions. The controller design should be able to interpret this feedback information to generate the actuator inputs. Generally, switching from constrained force control to unconstrained position control presents no problems. The opposite, however, has the significant problem of impact forces. The physical processes taking place during this phase are highly complex. Previous research has treated the impact phase as a transient that is dealt with by the same controller that follows some desired contact force command and in some way has ignored this important transitory period.

Matters get more complicated when flexibility of links or joints, that creates undesirable vibrational effects is present. While the high modes of the impact phenomena may be absorbed, allowing the controller more time to update the actuator input, extensive understanding of the dynamics of such flexible structures is required. For example, the naive control law which dictates *to move the arm till contact is achieved and then to apply the maximum torque in the opposite direction* may work for rigid manipulators but this is not the case for flexible ones, since inertia and flexibility contribute to negative acceleration at

the end-effector.

This thesis considers the problem of understanding the details of the impact phenomenon that takes place at the tip of a light-weight, single link, flexible robot arm. The final objective is to design a control system that passes the impact transient successfully and causes the manipulator to stably exert some desired force on the workpiece at the end. The single link flexible manipulator is obviously a distributed parameter system and therefore the first task is to choose a suitable approximate, finite dimensional model. A second order finite element approximation (i.e. the flexible link is represented by two rigid bodies coupled by revolute joints) is used throughout this work. The model is justified after comparisons between the simulation results and the experimental system response, prior to the design of the controller. Simulations include free beam motion prediction as well as constrained beam motion prediction.

The knowledge of the maximum impact force that will be developed at the arm tip on an impending contact event might be helpful, if not necessary, to correct the position controller while still in free space. The conventional and less accurate energy principle method is demonstrated in Chapter 4 , along with a much more efficient method based on the evaluation of instantaneous velocity increments immediately after contact.

The last chapter describes the real-time implementation of a hybrid impact-force controller. Previous schemes of impact control are briefly discussed and a

proposed impact-force control strategy is presented for the available experimental set-up. The second order finite element approximation is proven necessary, as computing power limitations and insufficient state measurements appear more acute in controlling such short transient events. It is useful to note that except for the case of the controller implementation, the work presented here can be be easily extended and improved by a higher order approximation.

Chapter 2

Experimental setup and modeling

2.1 Hardware description

The experimental setup consists of a single-link robot arm with link flexibility, an IBM PC-AT computer with A/D and D/A interface capabilities and three sensors. The flexible beam is excited by a DC brushless torque motor. The beam is mounted at the hub of the motor almost rigidly. In the mathematical analysis, however, the stiffness of this joint is taken into account. A collocated tachometer and an optical encoder measure the shaft angular velocity and displacement. The tip reaction force is measured using a noncollocated force sensitive resistor (FSR), manufactured by Interlink Electronics. The FSR element exhibits an electrical resistance which decreases with increasing normal pressure. Unlike strain gauges the change of FSR resistance is extremely large and follows a power law relationship. In terms of the time response the FSR can be considered a

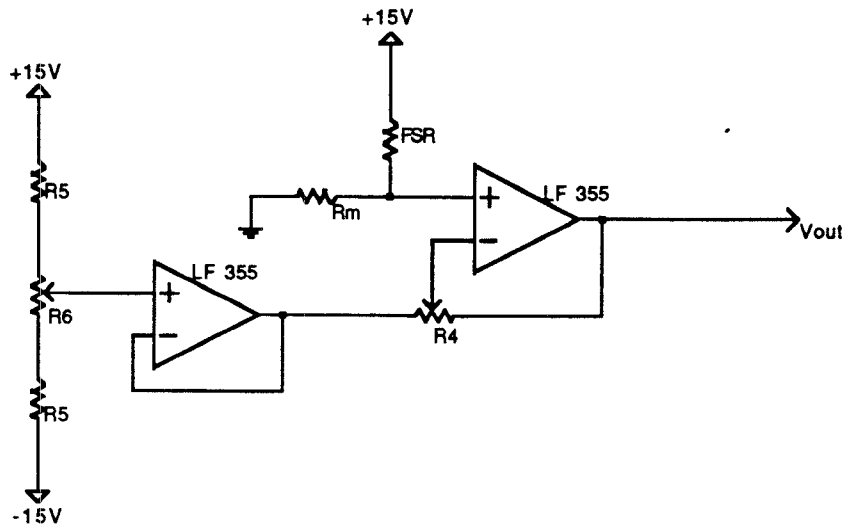

Figure 2.1: FSR interface circuit

slow device (unlike piezoelectric transducers) with typical mechanical rise time of 1-2 msec.

For a simple force-to-voltage conversion, the FSR is tied to a measuring resistor in a voltage divider configuration. The FET-input type op-amps LF 355 isolate the output signal from the high source impedance of the voltage divider and allow adjustment of the output offset and gain. The FSR interface circuit is presented in Figure 2.1. The values of R_M, R_5 and R_6 are $40K\Omega, 10K\Omega$ and $10K\Omega$ respectively. A more detailed description of the electronics which are installed for measuring angular position and velocity of the motor shaft, can be found in [1].

2.2 The beam and the contact model

The Euler-Bernoulli beam equation governing a flexible beam is a partial differential equation for a function of time and position along the beam and is thus a distributed parameter system. One method for solving such systems is to approximate the beam by a finite number of rigid elements which are connected by means of revolute joints. Posbergh, in [17] has shown that as the number of elements in the approximation approaches infinity, each solution converges to that of the continuum model.

The equations for the finite dimensional system constitute a Galerkin model of the beam. The model used to approximate the continuum model in our case was a three body approximation: one rigid body for the motor and the hub and two rigid bodies for the flexible beam. The rigid bodies are connected by rotary joints and coupled with torsional springs which depend linearly on the angle difference between the bodies. Let k_i be the spring constant of the ith joint. The center of mass of the ith body of the beam which has length l, lies at a point ϵ_i from the previous hinge. This rigid body is characterized by its mass m_i and the moment of inertia I_i about its center of mass.

Two methods for obtaining the equations of motion are : the Lagrangian and the Newton-Euler formulations. Here, we made use of the second method which is more suitable since it deals directly with external torques and forces

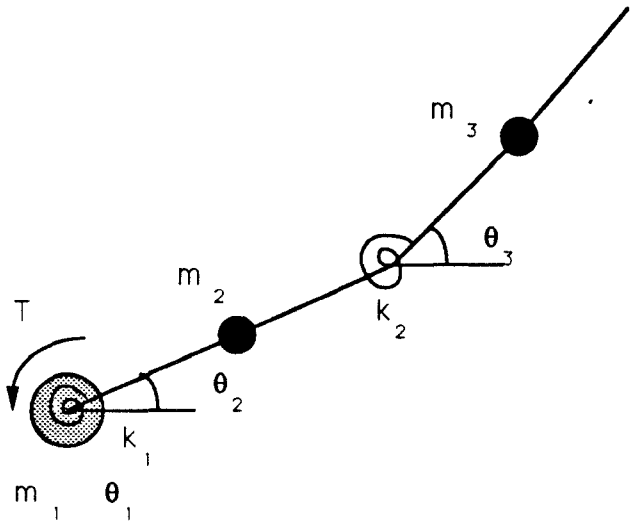

Figure 2.2: Finite Element Approximation

while the Lagrangian approach does so somewhat indirectly.

As far as the contact model is concerned, we assume *rigid, point frictionless contact.* The collisions taking place at the beam tip are ideally plastic (coefficient of restitution $e = 0$). Therefore, only an unknown reaction force will be present at the point of interaction instead of a general wrench. Moreover, given the flexibility and the dimensions of the beam, we may assume that the line of action of the reaction force f remains always normal to the third body of the finite element approximation.

If l_2 and l_3 are the angular momenta of the second and the third rigid bodies about the center of mass and the arbitrary torques and forces τ_1,τ_2,f_1,f_2 are as in Figure 2.3, then

$$\dot{\mathbf{l}}_2 = \tau_1 + \tau_2 + \mathbf{l} \times \mathbf{f}_2 \tag{2.1}$$

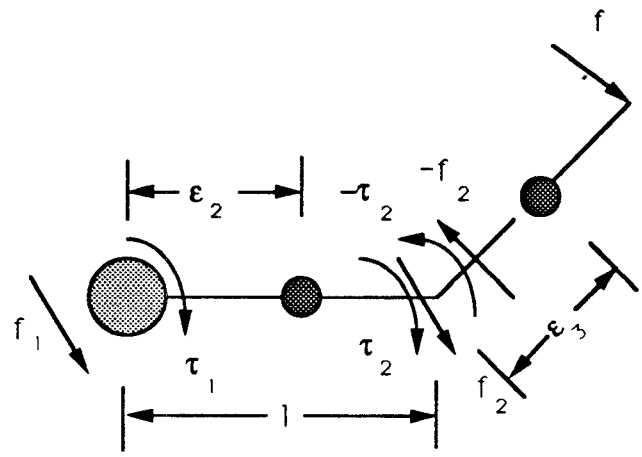

Figure 2.3: Torques and forces for the Newton-Euler approach

$$\dot{\mathbf{l}}_3 = -\tau_2 + \mathbf{l} \times (-\mathbf{f_2}) + \gamma \times \mathbf{f} \tag{2.2}$$

where γ is the tip position vector $[l(cos\theta_3 + cos\theta_2), l(sin\theta_3 + sin\theta_2, 0]^T$, in the reference coordinate system (of the first rigid body) and $\mathbf{l}$ is the position vector that corresponds to the second joint. From (2.1) and (2.2) by addition we get

$$\tau_1 = \dot{\mathbf{l}}_2 + \dot{\mathbf{l}}_3 - \gamma \times \mathbf{f}. \tag{2.3}$$

In the general case the Newton-Euler formulation gives $\dot{\mathbf{l}}$ which represents a torque as

$$\dot{\mathbf{l}}_\mathbf{i} = \dot{\mathbf{B}}_\mathbf{i}\mathbf{I}_\mathbf{i}\Omega_i + \mathbf{B}_\mathbf{i}\mathbf{I}_\mathbf{i}\dot{\Omega}_i + m_i(\mathbf{r_{0i}} \times \ddot{\mathbf{r}}_\mathbf{0i})$$

where $\mathbf{I_i}$ is the inertia tensor of the ith body about the center of mass expressed in the reference frame, $\mathbf{\Omega_i}$ is the rotational velocity expressed in the body frame and $\mathbf{B_i}$ is the homogenous transformation from the ith body frame to the base frame. Also $\mathbf{r_{0i}}$ is the position vector of the center of mass of the ith body in

the reference frame. Then $\dot{\mathbf{l}}_2$ and $\dot{\mathbf{l}}_3$ are given by

$$\dot{\mathbf{l}}_2 = \dot{\mathbf{B}}_2\mathbf{I}_2\Omega_2 + \mathbf{B}_2\mathbf{I}_2\dot{\Omega}_2 + m_2(\mathbf{r}_{02} \times \ddot{\mathbf{r}}_{02}) \tag{2.4}$$

$$\dot{\mathbf{l}}_3 = \dot{\mathbf{B}}_3\mathbf{I}_3\Omega_3 + \mathbf{B}_3\mathbf{I}_3\dot{\Omega}_3 + m_3(\mathbf{r}_{03} \times \ddot{\mathbf{r}}_{03}) \tag{2.5}$$

with

$$\mathbf{B}_2 = \begin{bmatrix} cos\theta_2 & -sin\theta_2 & 0 \\ sin\theta_2 & cos\theta_2 & 0 \\ 0 & 0 & 1 \end{bmatrix}$$

$$\mathbf{B}_3 = \begin{bmatrix} cos\theta_3 & -sin\theta_3 & 0 \\ sin\theta_3 & cos\theta_3 & 0 \\ 0 & 0 & 1 \end{bmatrix}$$

$$\mathbf{\Omega}_2 = [0, 0, \dot{\theta}_2]^T$$

$$\mathbf{\Omega}_3 = [0, 0, \dot{\theta}_3]^T$$

$$\mathbf{r}_{02} = [\epsilon_2 cos\theta_2, \epsilon_2 sin\theta_2, 0]^T$$

$$\mathbf{r}_{03} = [lcos\theta_2 + \epsilon_3 cos\theta_3, lsin\theta_2 + \epsilon_3 sin\theta_3, 0]^T.$$

Then the z-components (torques around the z-axis) of $\dot{\mathbf{l}}_2$ and $\dot{\mathbf{l}}_3$ are

$$\dot{l}_{2,z} = I_2\ddot{\theta}_2 + m_2\epsilon_2^2\ddot{\theta}_2 \tag{2.6}$$

$$\begin{aligned} \dot{l}_{3,z} &= (m_3l^2 + m_3l\epsilon_3cos(\theta_3 - \theta_2))\ddot{\theta}_2 + (I_3 + m_3\epsilon_3^2 + m_3l\epsilon_3cos(\theta_3 - \theta_2))\ddot{\theta}_3 \\ &+ m_3l\epsilon_3sin(\theta_3 - \theta_2)(\dot{\theta}_3^2 - \dot{\theta}_2^2) \end{aligned} \tag{2.7}$$

Now noticing that $\mathbf{f} = [f sin\theta_3, -f cos\theta_3, 0]^T$ where f is the amplitude of the external force,

$$\mathbf{f} \times \gamma = [0, 0, fl(1 + cos(\theta_3 - \theta_2)]^T.$$

If in (2.3) we include the torques arising from the springs then

$$\begin{aligned} k_2(\theta_3 - \theta_2) - k_1(\theta_2 - \theta_1) &= [m_2\epsilon_2^2 + m_3 l^2 + I_2 + m_3 l\epsilon_3 cos(\theta_3 - \theta_2)]\ddot{\theta}_2 \\ &+[m_3\epsilon_3^2 + I_3 + m_3 l e_3 cos(\theta_3 - \theta_2)]\ddot{\theta}_3 \\ &-m_3 l\epsilon_3 sin(\theta_3 - \theta_2)(\dot{\theta}_3^2 - \dot{\theta}_2^2) \\ &+fl[1 + cos(\theta_3 - \theta_2)]. \end{aligned}$$

For the third rigid body we have

$$\tau_2 = -\dot{\mathbf{l}}_3 + \mathbf{l} \times (-\mathbf{f_2}) + \gamma \times \mathbf{f} \tag{2.8}$$

Here we are making use of the Newton's equation for the third rigid body in order to derive an expression for $\mathbf{f_2}$

$$-\mathbf{f_2} + \mathbf{f} = m_3\ddot{\mathbf{r}}_{\mathbf{03}} \tag{2.9}$$

then (2.8) becomes

$$\begin{aligned} \tau_2 &= -\dot{\mathbf{l}}_3 + \mathbf{l} \times (m_3\ddot{\mathbf{r}}_{\mathbf{03}} - f) + \gamma \times \mathbf{f} \\ &= -\dot{\mathbf{l}}_3 + \mathbf{l} \times m_3\ddot{\mathbf{r}}_{\mathbf{03}} + (\gamma - \mathbf{l}) \times \mathbf{f} \end{aligned} \tag{2.10}$$

with $(\gamma - \mathbf{l}) = [lcos\theta_3, lsin\theta_3, 0]^T$. Including again the torsional terms we get

$$-k_2(\theta_3 - \theta_2) = m_3 l\epsilon_3 cos(\theta_3 - \theta_2)]\ddot{\theta}_2 + [m_3\epsilon_3^2 + I_3]\ddot{\theta}_3 + m_3 l\epsilon_3 sin(\theta_3 - \theta_2)\dot{\theta}_2^2) + fl$$

If the motor provides $T_{in}(t)$ torque on the shaft then easily

$$T_{in}(t) = I_1\ddot{\theta}_1 - k_1(\theta_2 - \theta_1).$$

The above equation has proved to be inconsistent with the experimental data, so it was updated using a comparatively accurate friction model for the motor which takes care of damping and kinetic friction,

$$T_{in}(t) = I_1\ddot{\theta}_1 - k_1(\theta_2 - \theta_1) + k_{fr}\dot{\theta}_1 + k_{st}sgn(\dot{\theta}_1). \tag{2.11}$$

For the motor the following equations hold

$$T_{in}(t) = k_T i(t) \tag{2.12}$$

$$R_a i(t) + k_B\dot{\theta}_1 = v(t) \Rightarrow i(t) = \frac{v(t) - k_B\dot{\theta}_1}{R_a}, \tag{2.13}$$

thus

$$T_{in}(t) = \frac{k_T}{R_a}v(t) - \frac{k_T k_B}{R_a}\dot{\theta}_1 \tag{2.14}$$

where R_a is the motor armature resistance, k_B is the motor back EMF constant and k_T is the motor torque constant. Summarizing, the nonlinear equations of motion that describe the constrained motion of the flexible arm, viewing the system with input as voltage rather than torque, are the following:

$$\frac{k_T}{R_a}v(t) = I_1\ddot{\theta}_1 - k_1(\theta_2 - \theta_1) + k_{fr}\dot{\theta}_1 + k_{st}sgn(\dot{\theta}_1) + \frac{k_T k_B}{R_a}\dot{\theta}_1 \tag{2.15}$$

$$k_2(\theta_3 - \theta_2) - k_1(\theta_2 - \theta_1) =$$

$$[m_2\epsilon_2^2 + m_3 l^2 + I_2 + m_3 l\epsilon_3 cos(\theta_3 - \theta_2)]\ddot{\theta}_2$$

$$+[m_3\epsilon_3^2 + I_3 + m_3 l\epsilon_3 cos(\theta_3 - \theta_2)]\ddot{\theta}_3$$

$$-m_3 l\epsilon_3 sin(\theta_3 - \theta_2)(\dot{\theta}_3^2 - \dot{\theta}_2^2) + fl[1 + cos(\theta_3 - \theta_2)] \tag{2.16}$$

$$\begin{aligned} -k_2(\theta_3 - \theta_2) &= m_3 l\epsilon_3 cos(\theta_3 - \theta_2)\ddot{\theta}_2 + (m_3\epsilon_3^2 + I_3)\ddot{\theta}_3 \\ &\quad + m_3 l\epsilon_3 sin(\theta_3 - \theta_2)\dot{\theta}_2^2 + fl \end{aligned} \tag{2.17}$$

2.3 The physical parameters of the system

Before proceeding with numerical and the experimental results, let us first describe the system's physical characteristics. The hub mass and inertia are computed from the hub's dimensions. The hub has radius $r = 11cm$, height $h = 0.87cm$ and it is made of aluminum which has density $26.6 \times 10^3 N/m^3$. Thus, the mass density is $\rho_{Al} = 26.6 \times 10^3/9.806 = 2.71 \times 10^3 Kg/m^3$. The total mass is computed as $m_1 = \rho_{Al}\pi r^2 h = 0.86Kg$ and its inertia is computed as $I_1 = m_1 r^2/2 = 5.2 \times 10^{-3} Kgm^2$. The mass of the second and the third link are computed from the mass density and the physical dimensions of the beam. The beam has width $w = 0.30625cm$, height $h = 4.826cm$ and length $L = 1m$. Therefore, $m_2 = m_3 = 0.20054Kg$. The inertia of the approximating rigid bodies of the beam is given by

$$I_2 = I_3 = \frac{\rho_{Al} hw}{24} = 1.67 \times 10^{-5}$$

k_B	$2.443V/(rad/sec)$
k_T	$0.249092Kgm/A$
R_a	33.6Ω
k_{fr}	$5.4192 \times 10^{-3}Nm/(rad/sec)$
k_{st}	$0.045Nm$

Table 2.1: Physical parameters of the DC brushless motor

The stiffness of the first torsional spring between the hub and the beam is

$$k_1 = 1.5 \times 10^6 \frac{lbin}{rad} = 1.5 \times 10^6 \times 9.806(1/2.2046)(1/39.37) = 169468.0882 \frac{Nm}{rad}.$$

The stiffness k_2 of the beam was found to be $k_2 = 4.92Nm/rad$ (see [17]). Given the dimensions of the beam and assuming uniform mass distribution, the Galerkin model parameters ϵ_2 and ϵ_3 are both taken equal to $0.25m$. The physical parameters of the DC brushless torque motor are presented in Table 2.1.

Note also that in the actual system there exists a power amplifier unit of nominal gain $k = 6.02$. The input to this unit which is driven by the PC interface has maximum rating $\pm 10V$.

2.3.1 Empirical system response

The experimental hardware incorporates an optical shaft encoder to measure angular displacement and a tachometer to measure the angular velocity of the motor shaft, i.e. of the first body of the approximation. No sensors are available for the remaining states of the system. Notice that given the high stiffness

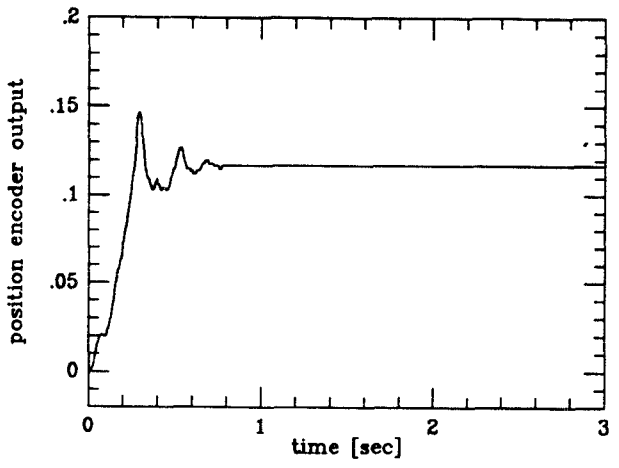

Figure 2.4: Optical encoder output

in the coupling between the hub and the beam, the states $(\theta, \dot{\theta}, \ddot{\theta})$ of the first and the second rigid bodies are almost identical. Figures 2.4, 2.5 and 2.6 show sample profiles from the optical encoder, the tachometer and the force transducer respectively for a continuous input of 10% of the maximum torque of the motor. The impact takes place at $0.1rad$ angle from the reference position. We assume that the beam collides with a single rigid body of infinite mass such as a rigid wall. The absolute velocity of this body remains zero throughout the experiment. The figures clearly indicate the various phases of the sample experiment:

- Motion in free space (reaction force is zero).
- Time instant of initial contact (instantaneous velocity increments).
- Discontinuity-free impact response which depends on the system dynamics.
- Loss of contact - bouncing.
- Steady-state phase (application of some constant tip force).

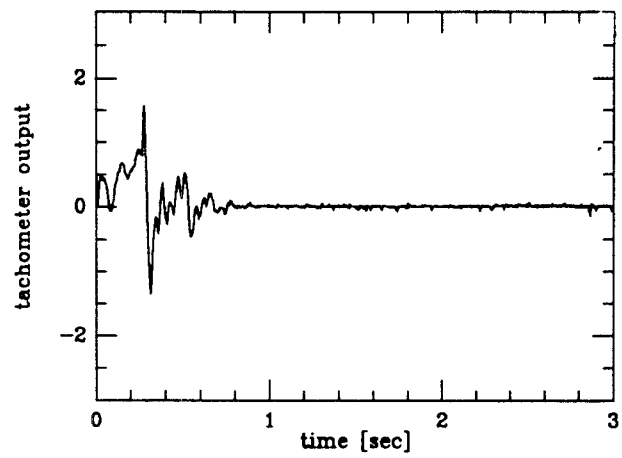

Figure 2.5: Tachometer output

The force output profile is to be understood as being more or less qualitative between the time instants of initial contact and steady-state phase, since the FSR (Force Sensing Resistor) sensor is unable to respond to this kind of high-frequency excitation. The use of a completely different type of sensor such as a piezoelectric sensor, and some noise reduction circuitry might improve the sensor output. However, we should keep in mind that the output of most common force transducers, including piezoelectric and strain-gauge type, goes off-scale in the impact phase. Consequently, the force output during this time period does not convey dependable information to be used for feedback.

The above profiles are available for comparison with the numerical results that follow in the next chapter.

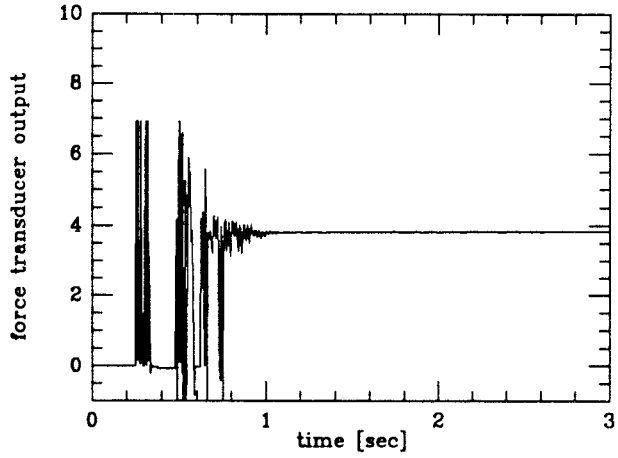

Figure 2.6: FSR output

Chapter 3

Model validation using a numerical approach

3.1 Description of the numerical problem

The system of equations (2.15),(2.16),(2.17) that describes the motion of the beam is nonlinear and closed form analytical solutions are unobtainable. It is therefore necessary to obtain suitable numerical approximations to the unknown angular displacements, velocities and accelerations. The Newmark family of integration methods is perhaps the most widely used family for solving this type of equations describing the dynamics of rigid body assemblies. The Newmark family contains as special cases several well-known numerical schemes. Therefore, the next section is devoted to a review of the Newmark algorithm. A more detailed description of the algorithm can be found in [15].

3.1.1 The Newmark approximation

We assume that the dynamic behavior of a rigid body system may be written as a family of n differential equations given by

$$M\ddot{x}(t) + P(\dot{x}(t), x(t)) = F(t), \qquad x(0) = x_0, \quad \dot{x}(0) = \dot{x}_0$$

where $x(t)$ is a $N \times 1$ vector of system displacements, M is an $N \times N$ mass-type matrix, P is a general $N \times 1$ vector depending on velocities and displacements of the system and $F(t)$ is an $N \times 1$ vector of forces applied at the global degrees of freedom.

The Newmark integration method approximates the response of nonlinear 2-nd order equations by making the assumption that the balance laws should be satisfied at every discretization instant. Moving to discrete dynamics for two consecutive time steps we have

$$M\ddot{x}_n + P(\dot{x}(t_n), x(t_n)) = F_n \tag{3.1}$$

$$M\ddot{x}_{n+1} + P(\dot{x}(t_{n+1}), x(t_{n+1})) = F_{n+1}. \tag{3.2}$$

Now assume that (3.1) has already been solved. We are interested in solving (3.2) for $t \in [t_n, t_{n+1}]$ given the state $(x_n, \dot{x}_n, \ddot{x}_n)$ as the initial condition. Since the number of equations is N, while the number of the unknowns is $3N$, some

relationships between accelerations, velocities and displacements should be employed in order to solve the problem. In general

$$\dot{x}(t) = \dot{x}(t_n) + \int_{t_n}^{t} \ddot{x}(\tau)d\tau, \qquad t \in [t_n, t_{n+1}]$$

$$x(t) = x(t_n) + \int_{t_n}^{t} \dot{x}(\tau)d\tau, \qquad t \in [t_n, t_{n+1}]$$

The main point of the Newmark method is that it makes reasonable assumptions about the change of the acceleration between the discretization time instants, while insisting on maintaining equilibrium at t_n and t_{n+1}. There are several possible implementations. For example, assume that the acceleration vector $\ddot{x}(t)$ is a linear combination of the boundary values $\ddot{x}(t_n)$ and $\ddot{x}(t_{n+1})$,

$$\ddot{x}(t) = (1-\gamma)\ddot{x}(t_n) + \gamma\ddot{x}(t_{n+1}), \qquad t \in [t_n, t_{n+1}] \tag{3.3}$$

where γ is some prescribed constant. From the above we obtain

$$\dot{x}(t) = \dot{x}(t_n) + [(1-\gamma)\ddot{x}(t_n) + \gamma\ddot{x}(t_{n+1})](t - t_n) \tag{3.4}$$

$$x(t) = x(t_n) + \dot{x}(t_n)(t - t_n) + [(1-\gamma)\ddot{x}(t_n) + \gamma\ddot{x}(t_{n+1})]\frac{(t-t_n)^2}{2} \tag{3.5}$$

Substituting the above equations in (3.2) we end up with a system of N equations with N unknowns, namely the vector $\ddot{x}(t_{n+1})$. Recasting $\ddot{x}(t_{n+1})$ into (3.3),(3.4),(3.5) the state of the system is completely determined. The general Newmark family that includes the above case is summarized below:

$$\dot{x}(t_{n+1}) = \dot{x}(t_n) + h[(1-\gamma)\ddot{x}(t_n) + \gamma\ddot{x}(t_{n+1})] \tag{3.6}$$

$$x(t_{n+1}) = x(t_n) + h\dot{x}(t_n) + h^2(\frac{1}{2} - \beta)\ddot{x}(t_n) + h^2\beta\ddot{x}(t_{n+1}), \tag{3.7}$$

where h is the time step $(t_{n+1} - t_n)$. Notice that instead of solving for the accelerations for the next time step, we can solve for either displacements or velocities once the relationships between the three vectors have been established.

The determination of the truncation errors, the accuracy of the method and the stability matters are beyond the scope of this review and they can be found in [15]. However, we recall some key results.

Remark: The stability and the accuracy of the method depends on β and γ parameters and on time step as well. A summary of the stability conditions for the general Newmark method is given in Table 3.1.

Unconditional	$2\beta \geq \gamma \geq 1/2$
Conditional	$\gamma \geq 1/2, \beta < \gamma/2, \omega^h h \leq \Omega_{crit}$

Table 3.1: Stability conditions of Newmark method

ω^h is the maximum natural frequency of the system and Ω_{crit} is the critical sampling frequency given by $\Omega_{crit} = (\gamma/2 - \beta)^{-1/2}$ for the undamped case. Therefore, the trapezoidal rule $(\beta = 0.25, \gamma = 0.5)$ is unconditionally stable while the linear acceleration method $(\beta = 1/6, \gamma = 0.5)$ is conditionally stable with $\Omega \simeq 3.464$. The accuracy of these methods is of 2nd order provided $\gamma = 0.5$.

Of great interest is the high frequency behavior of the Newmark method, since higher modes are artifacts of the impact phenomena. Therefore, it is generally viewed as desirable and often it is considered necessary to have some form

of algorithmic damping present to remove the high frequency components. For the Newmark method, $\gamma > 0.5$ is necessary to introduce high frequency dissipation. Also for some fixed γ, a particular value of β maximizes the dissipation. Unfortunately $\gamma \neq 0.5$ results in a drop to 1st order accuracy.

3.1.2 Numerical solution of the unconstrained motion of the beam

The equations of motion (a system of ordinary differential equations) are discretized using the above described Newmark algorithm. The nonlinear, algebraic system of equations that arises, has to be solved for either accelerations, velocities or displacements. There are no good general methods for solving systems of more than one nonlinear equation. Almost always we have to use additional information specific to the particular problem to answer questions about uniqueness etc. However, if we identify a neighborhood of a root, the Newton-Raphson method gives a very efficient means of converging to the root, if it exists, provided a good initial guess was used. Generally the object is to determine a vector $\mathbf{x} = [x_1, x_2, ...x_n]$ such that the functions $f_i(x_1, x_2, ...x_n)$, where $i = 1, 2, ...n$, are approximately zero. In the neighborhood of $\mathbf{x}$ each function f_i can be expanded in Taylor series:

$$f_i(\mathbf{x} + \delta\mathbf{x}) = f_i(\mathbf{x}) + \sum_{j=1}^{n} \frac{\partial f_i}{\partial x_j} \delta x_j + O(\delta\mathbf{x}^2).$$

By neglecting terms of $\delta\mathbf{x}^2$ order and higher we obtain a set of linear equations for the corrections $\delta\mathbf{x}$ that force the functions $f_i(\mathbf{x}+\delta\mathbf{x})$ to be zero simultaneously:

$$\mathbf{J}\delta\mathbf{x} = -\mathbf{f}(\mathbf{x}), \tag{3.8}$$

where $\mathbf{J}$ is a square matrix of partial derivatives $(\partial f_i/\partial x_j)$ and is called the Jacobian. Now (3.8) is a linear system of equations which can be easily solved given that $det(\mathbf{J}) \neq 0$. The corrections are then added to the solution vector:

$$\mathbf{x}^{\mathbf{new}} = \mathbf{x}^{\mathbf{old}} + \delta\mathbf{x}$$

and the process is iterated to convergence.

The routine *mnewt(ntrial,x,n, tolx,tolf)* of the package Numerical Recipes [21] performs this job for *ntrial* iterations starting from an initial guess x. Here n is the order of the system and *tolx* and *tolf* are tolerances for a stopping rule.

The above tools (the Newmark approximation along with the Newton Raphson method) were employed to solve the nonlinear system of equations (2.15), (2.16), (2.17) where $f = 0$ for the unconstrained case. Initially, the well known trapezoidal rule was proven to be sufficient to describe the free motion of the beam in terms of displacements and velocities. However, some rearrangement of β parameter was required for high frequency dissipation in the blurry and poor acceleration profiles. Velocity and displacement plots remained the same for various β within the stability region $2\beta \geq \gamma$. Values of $\gamma = 0.5$ and $\beta = 0.4$

were considered suitable throughout the numerical experiments. This value of γ maintains the 2nd order accuracy even though it does not provide high frequency dissipation. Time steps of the order of $10^{-2}sec$ up to $10^{-3}sec$ are adequate for the unconstrained motion.

Remark: In using the Newton-Raphson method to solve the nonlinear system, we note that a good initial guess for the angular displacement vector is dictated by the angular displacements of the previous time step. As soon as the beam follows a *continuous* trajectory with no impact phenomena present, the state of the previous time step should always lie in the neighborhood of the current state. The smaller the time step h gets, the smaller the difference $\Delta\theta$ from the previous time step and the higher the degree of convergence to the root.

3.1.3 Numerical results for the constrained motion of the beam

By the time contact is established at the tip of the beam, one more unknown, namely the amplitude of the reaction force, is present. Therefore, one more equation must be enforced. Recall that a contact problem is actually a *constraint problem.* The primary kinematic axiom of a contact problem is, that the

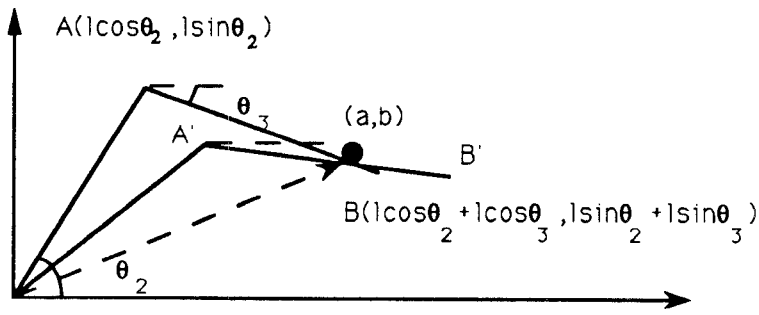

Figure 3.1: Configuration of the beam in contact

structures involved do not penetrate each other. Figure 3.1 shows the configuration of the beam in two consecutive states while contact is established[1]. The kinematic constraint is determined by the fact that the contact point should always belong to the line aligned to the third rigid body. If the coordinates of the contact point are (a, b) then *the numerical kinematic constraint* is given by:

$$tan\theta_3 = \frac{lsin\theta_3}{lcos\theta_3} = \frac{b - lsin\theta_2}{a - lcos\theta_2}$$

which implies,

$$asin\theta_3 - bcos\theta_3 - lsin(\theta_3 - \theta_2) = 0. \tag{3.9}$$

Therefore, the constrained motion of the beam is described by the dynamic

[1]Note here, that the contact point moves with respect to the coordinate frame of the third body of the approximation. However, the travel of the contact point is negligible for the given beam flexibility. Additionally, recall that this motion is assumed to be frictionless.

equations (2.15), (2.16), (2.17) and the algebraic kinematic constraint (3.9). Using again the Newmark approximation with $\gamma = 0.5$ and $\beta = 0.4$ along with the Newton-Raphson method, we are moving back and forth from a 3-dimensional system of equations to a 4-dimensional one. The transitions are primarily determined by the kinematic constraint. Additional numerical constraints correct possible truncation errors. The first results of this method were consistent as far as displacement and velocity were concerned, but this was not the case for the acceleration and force. Moreover, force plots were affected by the time step changes. Notice that we already expected a poor acceleration profile since the Newmark approximation for the acceleration variation inside the time steps was used. The method worked sufficiently well after a good choice of β for the free motion, but here high-frequency impact phenomena are involved. The velocity and displacement plots of the first and the third body are presented in Figures 3.2 and 3.3. The parameters used are time step of $0.001sec$, $\beta = 0.4$, $\gamma = 0.5$ and constant input voltage of $1V$. Bear in mind that given the high stiffness coupling between the hub and the beam, similar plots for the second body of the Galerkin approximation hold.

Generally, force and acceleration are closely related therefore , any problems in the acceleration plots will be transferred to the force plot. This can be also seen as follows. Let us take the integral in equation (2.17) from the moment

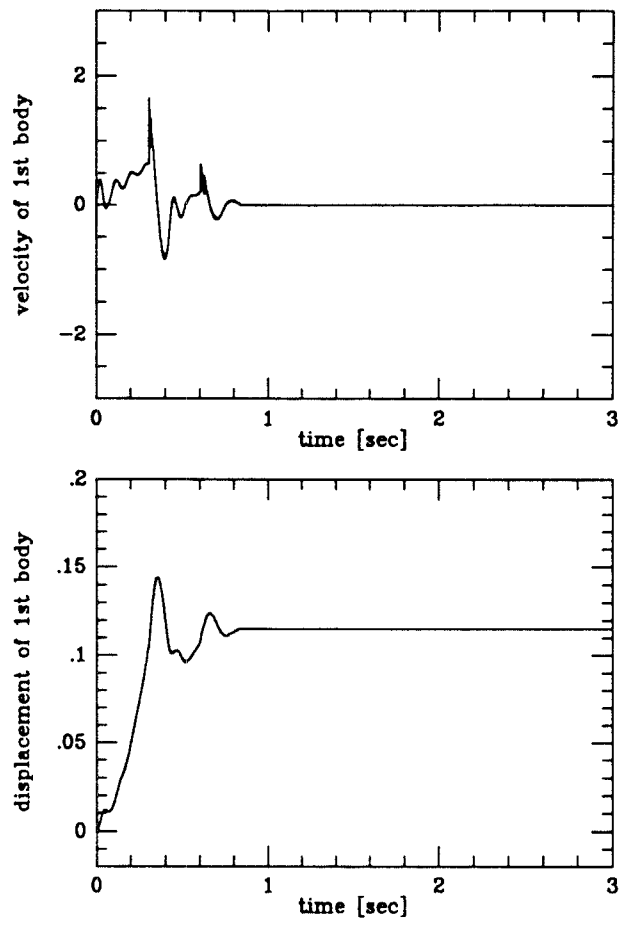

Figure 3.2: Velocity and displacement profile of the first body using step of $0.001sec$, $\beta = 0.4$, $\gamma = 0.5$ and voltage input $1V$

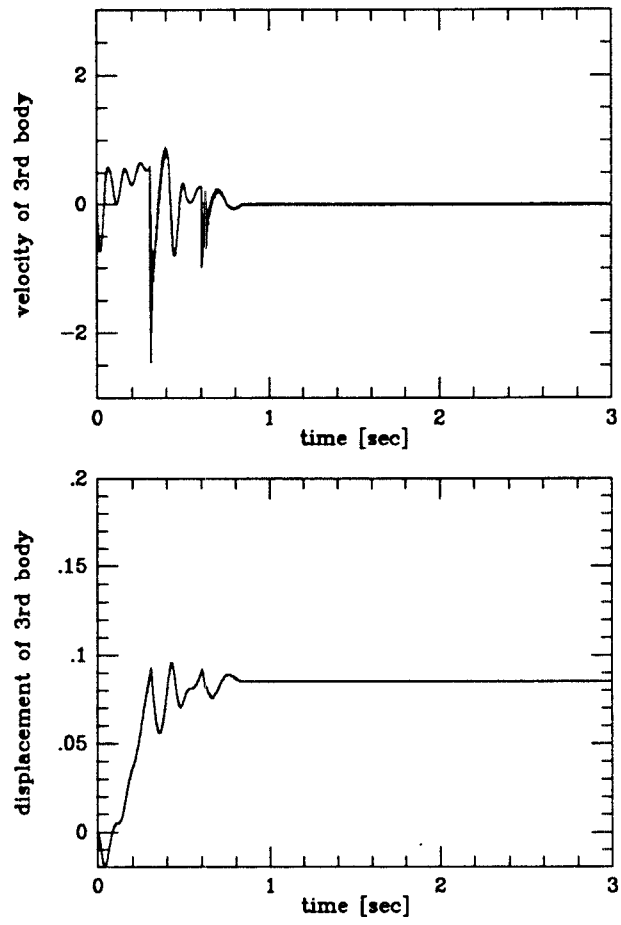

Figure 3.3: Velocity and displacement profile of the third body using step of $0.001sec$, $\beta = 0.4$, $\gamma = 0.5$ and voltage input $1V$

just before impact t_0 up to $t_0 + \Delta t$ and let Δt go to zero.

$$-\int_{t_0}^{t_0+\Delta t} k_2(\theta_3 - \theta_2)dt = \int_{t_0}^{t_0+\Delta t} fldt + \int_{t_0}^{t_0+\Delta t} m_3 l\epsilon_3 cos(\theta_3 - \theta_2)\ddot{\theta}_2 dt$$
$$+\int_{t_0}^{t_0+\Delta t} [m_3\epsilon_3^2 + I_3]\ddot{\theta}_3 dt + \int_{t_0}^{t_0+\Delta t} m_3 l\epsilon_3 sin(\theta_3 - \theta_2)\dot{\theta}_2^2)dt \qquad (3.10)$$

As it will be shown in the next chapter, during the short time interval that impact lasts, the position of all rigid bodies remain unchanged since all angular velocities remain finite. Springs, dampers and similar elements in the hinges do not play any role since they exert wrenches of finite magnitude. Only impulsive forces and torques can cause instantaneous velocity increments.

Definition: A force $f(t)$ is called an impulsive force, if the integral

$$\int_{t_0}^{t_0+\Delta t} f(t)dt$$

converges to a finite quantity $\hat{f}$ when Δt tends to zero.

Therefore, from equation (3.10) above we get

$$0 = m_3 l\epsilon_3 cos(\theta_3 - \theta_2)\int_{t_0}^{t_0+\Delta t} \ddot{\theta}_2 dt + [m_3\epsilon_3^2 + I_3]\int_{t_0}^{t_0+\Delta t} \ddot{\theta}_3 dt + \hat{f}l \qquad (3.11)$$

(the $\dot{\theta}_2^2$ term remains finite so that in the limit the integral is zero) this means that during impact, accelerations and forces are closely related. A more detailed analysis of impact problems in multi-body systems presented in the next chapter, clarifies the above assertions.

Even though we do not care too much about accelerations, we do care about the force. A first handy solution for improving the force plot is to introduce

high frequency dissipation by forcing $\gamma > 1/2$. This pushes the system in the conditional stability region and reduces accuracy to 1st order. Therefore, a smaller time step h should be picked. A program that scans the spectrum of possible values for β and γ while keeping the time step under reasonable limits (e.g.10^{-5}) was developed. Under these conditions no pair of β and γ gave acceptable stable results.

Note that high frequency problems arise not only from the Newmark method, but also from the numerical differentiation in the Newton-Raphson solution. It is well known that the Newton-Raphson method will spectacularly fail to converge if the initial guess is not good enough. And this is the case here since force experiences sudden changes in short periods of time.

However, given that the Newmark method is quite efficient for angular velocities and displacements as it is established by comparisons with the experimental data (compare Figures 2.4 and 2.5 with Figure 3.2), another method is proposed here in order to find the *true* accelerations and the reaction force.

Strategy: *At each time step while contact is established* we allow two different numerical runs. The first, using the Newmark approximation along with the Newton-Raphson method for solving the nonlinear system that arises, provides the vectors θ and $\dot{\theta}$. With the second running, we recast θ and $\dot{\theta}$ back in the constrained system of equations (2.15), (2.16), (2.17). Taking the derivative

with respect to time of the kinematic constraint equation twice, we get

$$lcos(\theta_3 - \theta_2)\dot{\theta}_2 + (acos\theta_3 + bsin\theta_3 - lcos(\theta_3 - \theta_2))\dot{\theta}_3 = 0 \tag{3.12}$$

and

$$lcos(\theta_3 - \theta_2)\ddot{\theta}_2 + (acos\theta_3 + bsin\theta_3 - lcos(\theta_3 - \theta_2))\ddot{\theta}_3 = 2lsin(\theta_3 - \theta_2)\dot{\theta}_2\dot{\theta}_3$$

$$-lsin(\theta_3 - \theta_2)\dot{\theta}_2^2 - (-asin\theta_3 + bcos\theta_3 + lsin(\theta_3 - \theta_2))\dot{\theta}_3^2 \tag{3.13}$$

Recall that during the infinitesimally short time interval that impact lasts, the positions of all rigid bodies do not change since all velocities remain finite. Therefore, displacements are continuous functions of time and there is no problem present in the first differentiation. However, the impulsive reaction force present at the tip can cause instantaneous velocity increments of finite magnitude. One should keep in mind, that at least theoretically acceleration reaches infinity at the time instant of initial contact.

Now, at each time step during contact, the acceleration vector $\ddot{\theta}$ and the reaction force should satisfy (2.15), (2.16), (2.17) and (3.13) as well. Therefore, we obtain a linear system of equations with unknowns $\ddot{\theta}$ and f. A simple matrix inversion solves the problem. The algorithm is summarized in Table 3.2, while the corresponding C code can be found in the Appendix. The results are presented in Figures 3.4 and 3.5 where a continuous input of 10% of the maximum torque of the motor is applied. The impact takes place at $0.1rad$ angle from the equilibrium position just as in the experimental case (see Chapter 2).

1	initialize displacement, velocity and acceleration vectors
2	if contact was not established in the previous time step, check if the current displacement vector satisfies the contact condition (3.13)
2.1	if the condition is still not satisfied solve the 3-dim nonlinear system that arises from the Newmark approximation and update the vectors
2.2	if the condition is satisfied, solve the 4-dim nonlinear system (using the kinematic constraint); substitute the resulting velocity and displacement vectors back to the initial equations and solve the *linear* 4-dim system (using the second derivative of the kinematic constraint); get the stable acceleration vector and reaction force; update vectors
3	if contact was already established in the previous step, check if the current displacement vector satisfies the release condition
3.1	if contact is still satisfied follow the procedure of step 2.2
3.2	if release condition is satisfied follow the procedure of step 2.1
4	repeat for the next time step

Table 3.2: Summary of the algorithm predicting the constrained beam motion

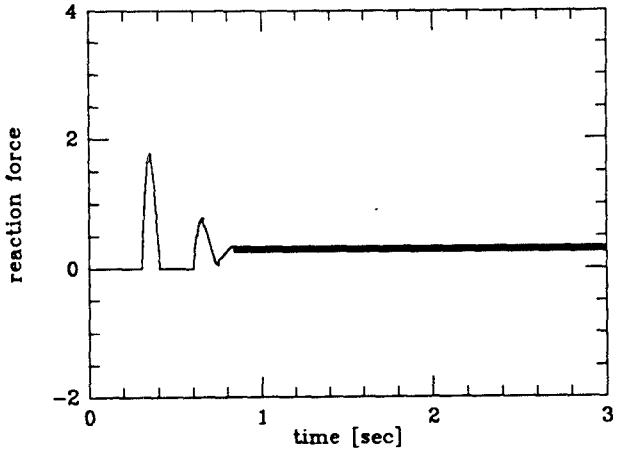

Figure 3.4: Reaction tip force profile using step of $0.001sec$, $\beta = 0.4$, $\gamma = 0.5$ and voltage input $1V$

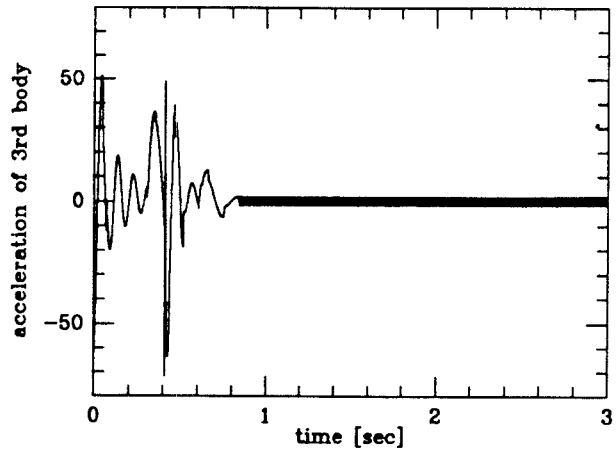

Figure 3.5: Acceleration profile of the third body using step of $0.001sec$, $\beta = 0.4$, $\gamma = 0.5$ and voltage input $1V$

Time steps of the order 10^{-3} or smaller are suggested for simulating the constrained motion of the beam. If this is the case, the numerical and the experimental results are surprisingly close given that the physical characteristics of the system and the position where the impact happens may include some errors.

Some quick observations can be made. A number of pulses in the reaction force precede the steady-state force. The beam bounces before it settles at the equilibrium position. The number of pulses and their duration depends mainly on the kinetic energy that is accumulated in the system (and consequently on the constant motor torque), as well as on the beam stiffness. In the limiting case where there is no flexibility at all, these pulses converge to delta functions, making the impact phenomenon impossible to control. Therefore, some amount of flexibility is deliberately desirable not only because it provides the system

with the necessary compliance to touch objects, but also because it grants the impact force controller with additional time to respond.

The maximum force occurs when the angular velocities of all bodies reach zero. From various experiments that were conducted, this maximum force seems to depend on the velocities just before impact, a factor that has found wide use in impact and force control in the past ([27]). Unfortunately, this qualitative observation is insufficient to solve the impact controller design problem since it ignores the dynamics of the impact, i.e. the type of the contact and the structure of the multi-body system that collides. More details will follow in the next chapter. For the sake of comparison, Figures 3.6-3.11 present the results of the method for various time steps and input voltages.

Remark 1: we do not claim that the Newmark approximation cannot solve the constrained motion problem. Simply, since high-frequency phenomena are involved, unacceptably small time steps should be used to avoid instability. Changing the value of γ to introduce high-frequency dissipation, a drop in the order of accuracy is inevitable as well. We should also emphasize that more sensitive impact and release conditions are necessary if one is to avoid taking excessively small time steps.

Remark 2: the numerical results presented in this chapter can be easily expanded using a higher order finite element approximation. As we noticed, the kinematic constraint reduced the degrees of freedom of the multibody chain

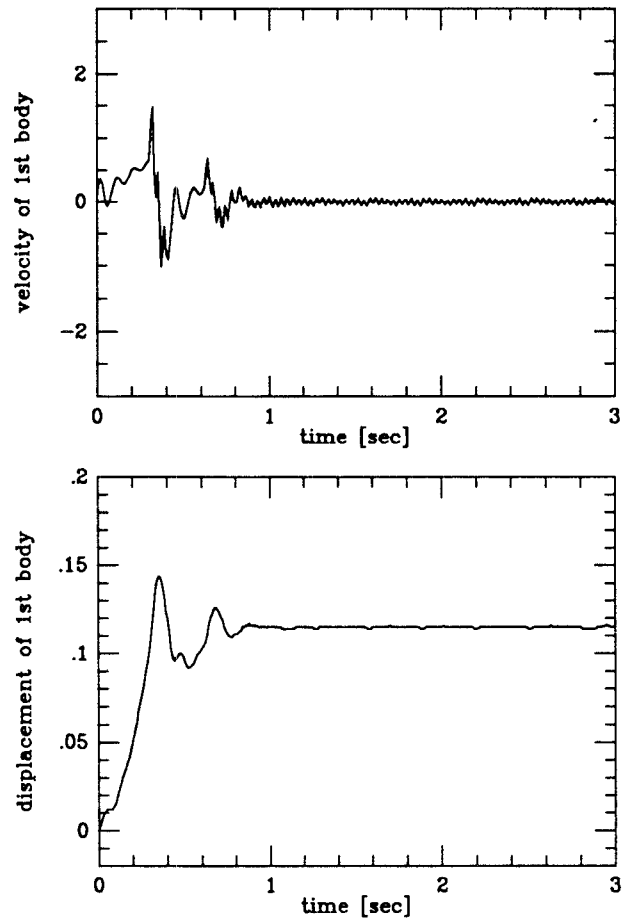

Figure 3.6: Velocity and displacement profile of the first body using step of $0.01sec$, $\beta = 0.4$, $\gamma = 0.5$ and voltage input $1V$

manipulator by one. In the case of an N-order approximation, we obtain $N+1$ equations (the additional equation refers to the hub body) and one kinematic constraint of the form $q(\theta_1, \theta_2, ...\theta_{N+1}) = 0$. Using the algorithm presented above, although the numerical complexity of the problem is increased, the solution is still feasible using no additional assumptions.

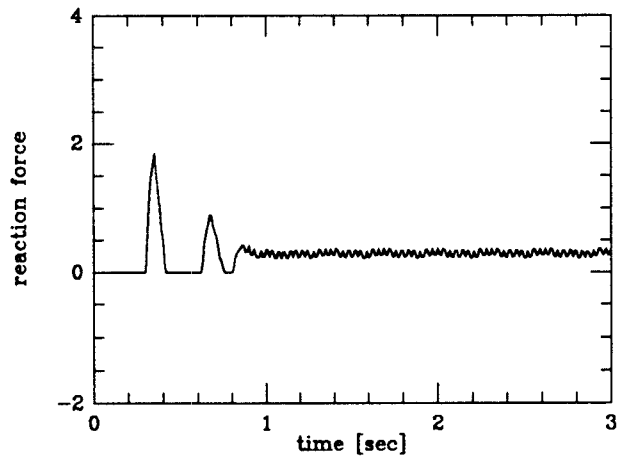

Figure 3.7: Reaction tip force profile using step of $0.01sec$, $\beta = 0.4$, $\gamma = 0.5$ and voltage input $1V$

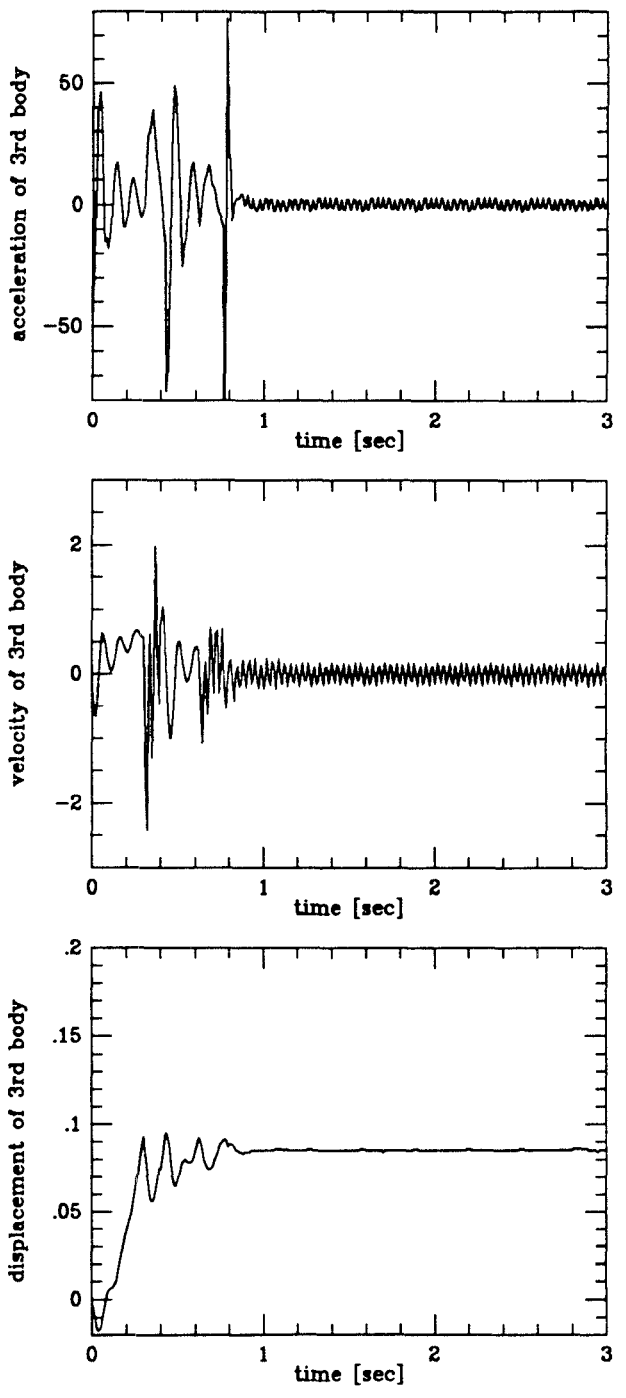

Figure 3.8: Acceleration, velocity and displacement profile of the third body using step of $0.01sec$, $\beta = 0.4$, $\gamma = 0.5$ and voltage input $1V$

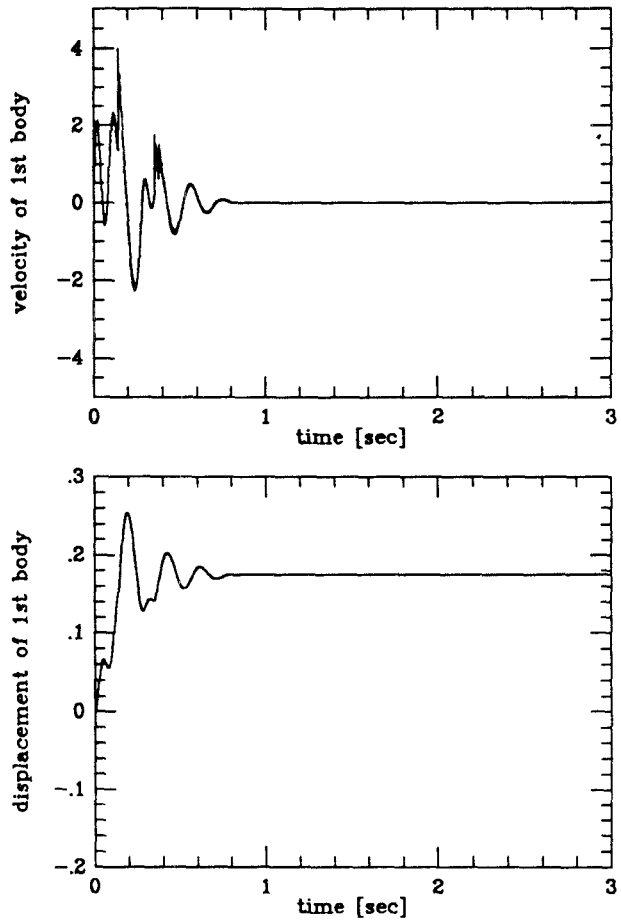

Figure 3.9: Velocity and displacement profile of the first body using step of $0.001sec$, $\beta = 0.4$, $\gamma = 0.5$ and voltage input $5V$

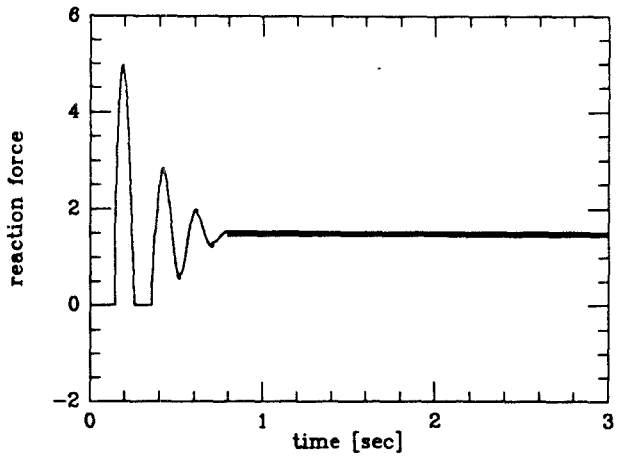

Figure 3.10: Reaction tip force profile using step of $0.001sec$, $\beta = 0.4$, $\gamma = 0.5$ and voltage input $5V$

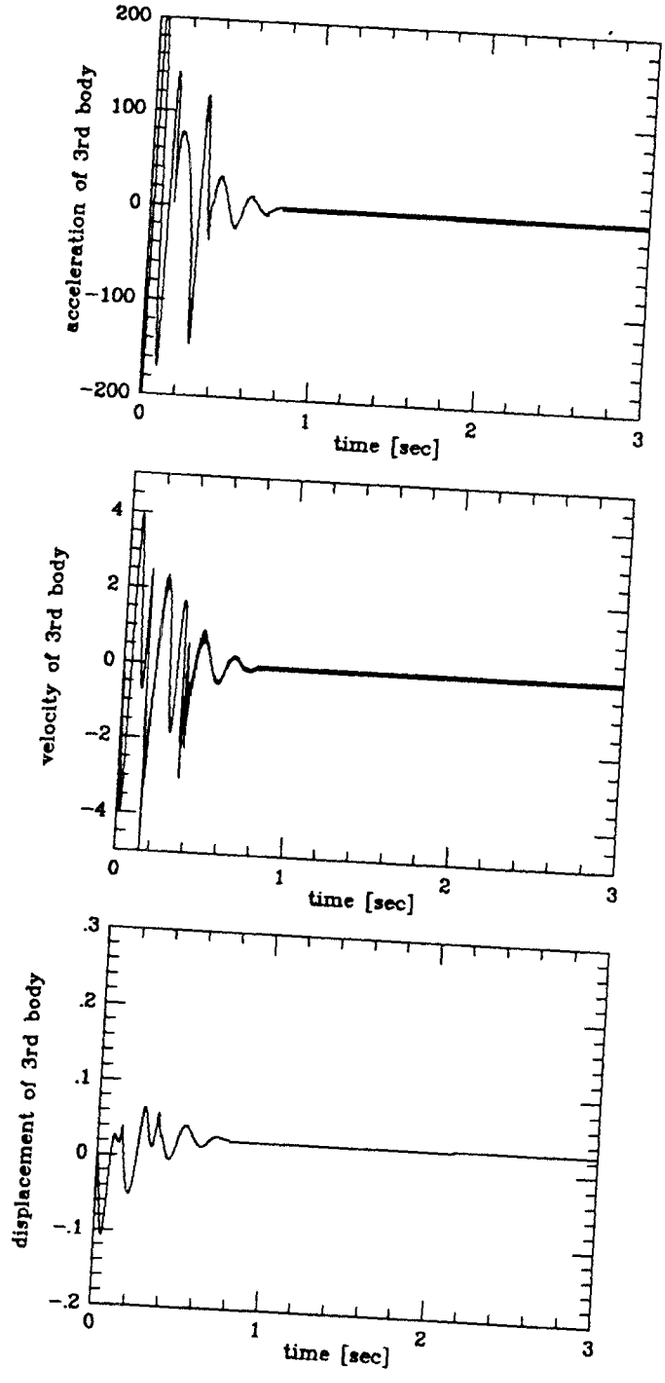

Figure 3.11: Acceleration, velocity and displacement profile of the third body using step of $0.001sec$, $\beta = 0.4$, $\gamma = 0.5$ and voltage input $5V$

Chapter 4

Prediction of the maximum reaction force

4.1 The maximum force prediction as an advantage of the impact controller

In the next chapter where the design problem of the impact-force controller is addressed, we shall see the importance of the ability to estimate the maximum reaction force[1] ahead of time. Obviously the most accurate way to proceed, is to solve the problem numerically. However, as was demonstrated in the previous

[1]We shall see in this chapter that a typical contact force profile is comprised of an initial delta function (which causes the instantaneous velocity increments), followed by a discontinuity-free portion. The importance of the impulsive part is completely theoretical since such event is neither physically captured nor controlled. In the sequel, the term maximum reaction force refers to the finite portion of the reaction force.

chapters, this involves comparatively long time delays for real-time implementations. In recent work the problem of finding closed form estimates of the maximum impact force was based exclusively on the energy principle ([16],[7]). This method seems to work sufficiently well for the simplified case of single-body collisions and for low-stiffness contacts. The alternate way that is proposed here is based on understanding of the impact phenomenon and it is restricted neither by the inherent characteristics of the bodies involved in the impact problem, nor by the complexity of the body-structure. The general questions addressed here, are:

1. Given the complete state of the system $(\theta, \dot{\theta}, \ddot{\theta})$ and some specified control law, is it possible to get an estimate of the maximum impact force that will be developed at the tip *if* contact is sensed in the very next time step?

2. What is the time interval between the initial contact and the time of maximum reaction force?

If we can answer these types of questions, then

1. we can avoid entering the unstable or the unable-to-respond region of the impact controller (for example, by reducing the impending contact velocity while still in free space) and

2. using a trial and error type method we can justify the control law that the impact controller proposes for diminishing the impact effect.

The conventional energy method, while it does not provide answers to all of the above questions and is not of much help in the impact controller design, will be demonstrated here for the sake of comparison.

4.1.1 Some basic assumptions on impact dynamics

The present subsection studies the discontinuous changes of velocities and angular velocities which a system experiences when impact takes place. Impact phenomena occur when a multi-body system collides with another multi-body system. The physical processes during impact are highly complex and some simplifying assumptions must be made in order to solve the mathematical problem that arises. Whether these are acceptable must be judged in each particular case. Extensive results on impact problems in holonomic multi-body systems can be found in [26].

In general, the impact phenomenon lasts a comparatively short time interval Δt, usually of the order of milliseconds in our flexible beam experiment. Wittenburg [26] in his analysis makes the assumption that in the mathematical description, the idealization $\Delta t \rightarrow 0$ is possible. This implies (and is implied) that any propagation of waves of deformation through bodies is neglected since such processes require finite periods of time to develop. Hence, the bodies of the system are treated as rigid bodies during impact. Since Wittennburg's analysis

assumes no compliance present in the hinges, the interaction between the colliding systems is completed in an infinitesimal amount of time. This is certainly not the case for our experiment. Even if we assume *rigid collisions* at the point of interaction, the flexibility of the beam spreads the impact effect in time. Delta functions of the impact force profile for the rigid body - rigid joint case become pulses of substantial duration for flexible-body systems. *Propagation of waves of deformations cannot be neglected.* But the analysis presented in [26] is useful to explain phenomena that take place at the time instant of initial contact (as $\Delta t \rightarrow 0$), e.g. instantaneous velocity increments etc. The dynamics along with the kinematic constraint take care of the smooth, discontinuity-free motion of the beam just after this time instant.

In this preliminary subsection we will concentrate only on what happens to the system over the infinitesimally short time interval just before and just after contact. During this interval the positions of all rigid bodies remain unchanged, since all velocities and angular velocities remain finite. Springs, dampers etc, exert forces and torques of finite magnitude whose integral over this infinitesimally short duration is zero. As was already mentioned, only impulsive forces and torques can cause discontinuous changes of velocities. We define the *impulse* as:

$$\hat{f} = \lim_{\Delta t \rightarrow 0} \int_{t_0}^{t_0+\Delta t} f(t)dt.$$

An impulsive torque similarly, is called *impulse couple.*

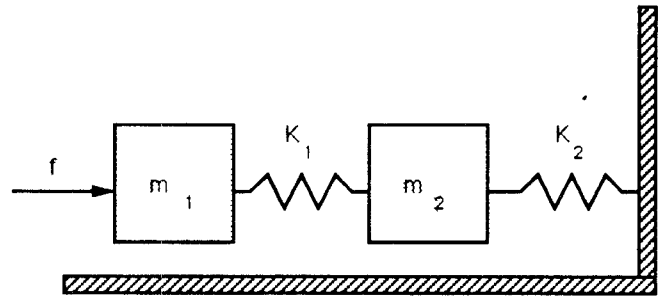

Figure 4.1: Lumped parameter spring-mass model for the beam experiment

Now depending on the nature of collision, elastic and/or plastic deformation may occur. However, we allow only ideally plastic deformation in the tip-object contact (coefficient of restitution $e = 0.0$) and consequently the colliding bodies have zero relative velocity at the point of collision immediately after impact as well as during the whole period that contact is maintained. This is because the kinetic energy that is imparted to the system by the collision is relaxed on beam deformation rather than on contact deformation. For convenience, imagine our system as springs connected in series as in Figure 4.1.

$$\frac{1}{k_{eq}} = \sum_{i=1}^{n} \frac{1}{k_i}$$

where $i = 2$ in our case. Since the stiffness k_1 is the largest, the beam bending gets virtually all the kinetic energy . If we still insist on characterizing the type of the collision through some coefficient of restitution we can define

$$e_{eq} = \frac{kinetic\ energy\ released\ during\ restitution}{elastic\ energy\ stored\ during\ collision\ in\ the\ beam\ stiffness}$$

where $e_{eq} \leq 1$. Therefore, we view the collision as having clearly separated compression and decompression phases which refer to the beam stiffness (not on

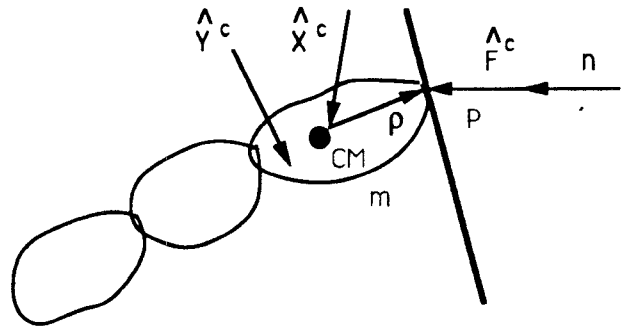

Figure 4.2: Body configuration during collision

a stiffness modeling the contact). We also assume that the impulsive interaction forces are directed normal to the common tangent plane at the point of collision. This means that there is no friction between the bodies and no tangential forces are present. Finally, we do not allow any play in the hinges.

4.1.2 Instantaneous velocity increments

With the assumptions specified in the previous subsection, the problem of impact is now reduced to the determination of two groups of mechanical quantities. One group is made up of the instantaneous velocity increments. The second group comprises external impulses at the point of collision. In order to get explicit solutions for the above quantities, the kinematics and the dynamics of the colliding bodies are required. For the present purposes, we assume that the second colliding system is a single rigid body of infinite mass, such as a rigid wall. The absolute velocity of this body remains zero throughout the experiment. A general impact set-up is shown in Figure 4.2. It does not matter to how many

contiguous bodies the colliding body is coupled. After all hinges are cut, some resulting force $\hat{\mathbf{X}}^{\mathbf{c}}$ and torque $\hat{\mathbf{Y}}^{\mathbf{c}}$ act on the terminal body. In general, $\hat{\mathbf{X}}^{\mathbf{c}}$ and $\hat{\mathbf{Y}}^{\mathbf{c}}$ are considered impulsive. At the point of collision the impulse $\hat{\mathbf{f}}$ is applied as well. Newton's second law and the law of moment of momentum for this body are the following

$$m\dot{v}_{\mathbf{c}} = \mathbf{F}^{\mathbf{c}}(t) + \mathbf{X}^{\mathbf{c}}(t) \tag{4.1}$$

$$\mathbf{J}\dot{\omega} + \omega \times \mathbf{J}\omega = \rho \times \mathbf{F}^{\mathbf{c}}(t) + \mathbf{Y}^{\mathbf{c}}(t) \tag{4.2}$$

Taking the integral over Δt and then the limit as $\Delta t \to 0$ we get

$$m\Delta v_{\mathbf{c}}^{\mathbf{c}} = \hat{\mathbf{F}}^{\mathbf{c}} + \hat{\mathbf{X}}^{\mathbf{c}} \tag{4.3}$$

$$\mathbf{J}\Delta\omega_{\mathbf{c}} = \rho \times \hat{\mathbf{F}}^{\mathbf{c}} + \hat{\mathbf{Y}}^{\mathbf{c}}. \tag{4.4}$$

Notice that the term $\omega \times \mathbf{J}\omega$ remains finite so that in the limit its integral is zero. The quantity $\Delta v_{\mathbf{c}}^{\mathbf{c}}$ is the finite increment of the absolute linear velocity of the body center mass and $\Delta\omega^{\mathbf{c}}$ is similarly the instantaneous increment of the angular velocity of the body. The point of collision P experiences a velocity increment equal to

$$\Delta v_{\mathbf{p}}^{\mathbf{c}} = \Delta v_{\mathbf{c}}^{\mathbf{c}} + \Delta\omega^{\mathbf{c}} \times \rho. \tag{4.5}$$

All this takes place immediately after the contact. One should bear in mind that during this short time Δt no change in body displacements is present. The dynamic equations (4.3) and (4.4) are linear equations with constant coefficients for the unknown velocity increments, impulses and impulse couples.

In a general setting, Wittenburg [26] showed that *the instantaneous velocity increments and impulses are related through linear equations with constant coefficients* in the case of ideal plastic collision and in the case of frictionless collision as well. These coefficients cannot be scalars since an equation of the form $\Delta v = a\mathbf{F}$, where a is a scalar, would imply that Δv has the direction of $\mathbf{F}$ and this is not generally true. Therefore a relation of the following type has to be considered

$$\Delta v = \mathbf{UF} \tag{4.6}$$

where $\mathbf{U}$ is a matrix with constant entries which depend only on the state of the system just before impact.

Therefore, by using (4.3) and (4.4) along with some kind of kinematic equations of the form of (4.5), we can evaluate the scalar magnitude of impulsive forces and torques, once the linear relationship (4.6) between instantaneous velocity increments and impulses is found. This relationship is provided by the differential equations of motion while the additional kinematic equation comes from our kinematic constraint (3.9) for the contact point. The procedure is summarized below.

Procedure: We assume that we know explicitly the positions and the velocities for all bodies involved in the process just before impact. We take the integral of the equations of motion from time t_0 just prior to impact, up to time $(t_0 + \Delta t)$ and we let $\Delta t \to 0$. Keeping in mind that all quantities that are

functions of generalized coordinates and of time remain the same before and after impact and consequently they are treated as constants, we obtain the desired relationship between the increment of generalized velocities (and angular ones) and the external impulses. *Some care should be taken in handling terms depending on generalized velocities* as we will see in the next section.

4.2 Impact dynamics of the flexible beam experiment

Now, let us apply the above stated procedures in our case. The desired relationships for angular velocity increments and the reaction impulse can be developed by the differential equations of continuous motion (2.15), (2.16), and (2.17) where f is considered to be impulsive. Following the above procedure we get

$$\begin{aligned}\int_{t_0}^{t_0+\Delta t} \frac{k_T}{R_a} v(t)dt &= \int_{t_0}^{t_0+\Delta t} I_1\ddot{\theta}_1 dt - \int_{t_0}^{t_0+\Delta t} k_1(\theta_2-\theta_1)dt \\ &+ \int_{t_0}^{t_0+\Delta t} [k_{f_r}\dot{\theta}_1 + k_{st}sgn(\dot{\theta}_1) + \frac{k_T k_B}{R_a}\dot{\theta}_1]dt \end{aligned} \tag{4.7}$$

$$\begin{aligned} 0 &= -\int_{t_0}^{t_0+\Delta t} k_2(\theta_3-\theta_2)dt + \int_{t_0}^{t_0+\Delta t} k_1(\theta_2-\theta_1)dt \\ &+ \int_{t_0}^{t_0+\Delta t} [m_2\epsilon_2^2 + m_3 l^2 + I_2 + m_3 l\epsilon_3 cos(\theta_3-\theta_2)]\ddot{\theta}_2 dt \\ &+ \int_{t_0}^{t_0+\Delta t} [m_3\epsilon_3^2 + I_3 + m_3 l e_3 cos(\theta_3-\theta_2)]\ddot{\theta}_3 dt \\ &- \int_{t_0}^{t_0+\Delta t} m_3 l\epsilon_3 sin(\theta_3-\theta_2)(\dot{\theta}_3^2 - \dot{\theta}_2^2)dt \end{aligned}$$

$$+\int_{t_0}^{t_0+\Delta t} fl[1+cos(\theta_3-\theta_2)]dt \tag{4.8}$$

$$\begin{aligned} 0 &= \int_{t_0}^{t_0+\Delta t} k_2(\theta_3-\theta_2)dt + \int_{t_0}^{t_0+\Delta t} fldt + \int_{t_0}^{t_0+\Delta t} m_3 l\epsilon_3 cos(\theta_3-\theta_2)\ddot{\theta}_2 dt \\ &+ \int_{t_0}^{t_0+\Delta t} [m_3\epsilon_3^2 + I_3]\ddot{\theta}_3 dt + \int_{t_0}^{t_0+\Delta t} m_3 l\epsilon_3 sin(\theta_3-\theta_2)\dot{\theta}_2^2 dt \end{aligned} \tag{4.9}$$

from these we get

$$0 = I_1[\dot{\theta}_1(t_0+\Delta t) - \dot{\theta}_1(t_0)] + (k_{fr} + \frac{k_T k_B}{R_a})[\theta_1(t_0+\Delta t) - \theta_1(t_0)] \tag{4.10}$$

$$\begin{aligned} 0 &= [m_2\epsilon_2^2 + m_3 l^2 + I_2 + m_3 l\epsilon_3 cos(\theta_3-\theta_2)]\Delta\dot{\theta}_2 \\ &+ [m_3\epsilon_3^2 + I_3 + m_3 l e_3 cos(\theta_3-\theta_2)]\Delta\dot{\theta}_3 + \hat{f}l[1+cos(\theta_3-\theta_2)] \end{aligned} \tag{4.11}$$

$$0 = m_3 l\epsilon_3 cos(\theta_3-\theta_2)\Delta\dot{\theta}_2 + [m_3\epsilon_3^2 + I_3]\Delta\dot{\theta}_3 + \hat{f}l \tag{4.12}$$

Equation (4.10) easily provides that the instantaneous velocity increment of the first body of the approximation is zero. This body experiences instantaneous velocity increment (see experimental as well as numerical results), but this occurs only after some finite period of time. In order to solve for the instantaneous velocity increments $\Delta\dot{\theta}_2$, $\Delta\dot{\theta}_3$ and $\hat{f}$ one more equation is needed. This equation as was mentioned previously comes from the kinematics. The kinematic constraint obviously holds just before and after the impact. But since it depends only on angular displacements which remain the same for $\Delta t \rightarrow 0$, it does not provide any additional information (i.e. it holds for both t_0 and $(t_0+\Delta t)$).

Equation (3.12) was used to provide the required kinematics equation. If θ_{i0} and $\dot{\theta}_{i0}$ are the angular displacements and the angular velocities of the bodies

just before impact, then we have for the time instant immediately after impact

$$\begin{aligned} 0 &= lcos(\theta_{30} - \theta_{20})(\dot{\theta}_{20} + \Delta\dot{\theta}_2) \\ &\quad +(acos\theta_{30} + bsin\theta_{30} - lcos(\theta_{30} - \theta_{20}))(\dot{\theta}_{30} + \Delta\dot{\theta}_3) \end{aligned} \tag{4.13}$$

From the above we can easily get

$$lcos(\theta_{30} - \theta_{20})\Delta\dot{\theta}_2 + (acos\theta_{30} + bsin\theta_{30} - lcos(\theta_{30} - \theta_{20}))\Delta\dot{\theta}_3 = \omega_0 \tag{4.14}$$

where ω_0 is defined by

$$\omega_0 = -lcos(\theta_{30} - \theta_{20})\dot{\theta}_{20} - (acos\theta_{30} + bsin\theta_{30} - lcos(\theta_{30} - \theta_{20}))\dot{\theta}_{30} \tag{4.15}$$

Equations (4.11), (4.12) and (4.14) comprise a system of linear equations, which can be easily solved for the instantaneous velocity increments and for the impulsive reaction force. In particular, from (4.11) and (4.12) we have (after a simple matrix inversion),

$$\begin{bmatrix} \Delta\dot{\theta}_2 \\ \Delta\dot{\theta}_3 \end{bmatrix} = \begin{bmatrix} m_3\epsilon_3^2 + I_3 & -(m_3\epsilon_3^2 + I_3 + m_3 l\epsilon_3 cos(\theta_{30} - \theta_{20})) \\ -m_3 l\epsilon_3 cos(\theta_{30} - \theta_{20}) & m_2\epsilon_2^2 + m_3 l^2 + m_3 l\epsilon_3 cos(\theta_{30} - \theta_{20}) \end{bmatrix}$$

$$\cdot \begin{bmatrix} 1 + cos(\theta_{30} - \theta_{20}) \\ 1 \end{bmatrix} \frac{-\hat{f}l}{\Delta}$$

where $\Delta = (m_2\epsilon_2^2 + m_3 l^2 + I_2)(m_3\epsilon_3^2 + I_3) - m_3^2 l^2 \epsilon_3^2 cos^2(\theta_{30} - \theta_{20})$

$$\begin{bmatrix} \Delta\dot{\theta}_2 \\ \Delta\dot{\theta}_3 \end{bmatrix} = \frac{-\hat{f}l}{\Delta} \begin{bmatrix} (m_3\epsilon_3^2 + I_3)cos(\theta_{30} - \theta_{20}) - m_3 l\epsilon_3 cos(\theta_{30} - \theta_{20}) \\ m_2\epsilon_2^2 + m_3 l^2 + I_2 - m_3 l\epsilon_3 cos^2(\theta_{30} - \theta_{20}) \end{bmatrix} \tag{4.16}$$

If we define v_0 as follows,

$$\begin{aligned} v_0 &= [acos\theta_{30} + bsin\theta_{30} - lcos(\theta_{30} - \theta_{20})][m_2\epsilon_2^2 + m_3l^2 - m_3l\epsilon_3cos^2(\theta_{30} - \theta_{20})] \\ &\quad + lcos(\theta_{30} - \theta_{20})[(m_3\epsilon_3^2 + I_3)cos(\theta_{30} - \theta_{20}) - m_3l\epsilon_3cos(\theta_{30} - \theta_{20})] \end{aligned}$$

then by substituting (4.16) in (4.14) we get

$$\hat{f} = -\frac{\omega_0\Delta}{lv_0} \tag{4.17}$$

where ω_0 and v_0 depend only on the the state of the system just before contact. Therefore, (4.17) gives the impulse that will be developed in the infinitesimal amount of time that the initial contact lasts. Substituting (4.17) back in (4.16), we get a closed form solution for $\Delta\dot{\theta}_2$ and $\Delta\dot{\theta}_3$. The new velocities immediately after impact for the second and the third bodies easily provide the following:

$$\dot{\theta}_2(t_0 + \Delta t) = \dot{\theta}_{20} + \Delta\dot{\theta}_2, \qquad \dot{\theta}_3(t_0 + \Delta t) = \dot{\theta}_{30} + \Delta\dot{\theta}_3 \tag{4.18}$$

Remarks: Intuitively, we expect that $\Delta\dot{\theta}_2$ and $\Delta\dot{\theta}_3$ should always be of different sign. Let us check if this is satisfied by our closed form solutions. Notice that since $\theta_2 \simeq \theta_3$, $cos(\theta_3 - \theta_2)$ is always positive (actually $-(\pi/2) \leq \theta_3 - \theta_2 \leq (\pi/2)$). Also $\epsilon_2 = \epsilon_3 = \epsilon = (l/2)$ and $m_2 = m_3 = m$.

$$[m\epsilon^2 + I_3 - ml\epsilon]cos(\theta_3 - \theta_2) \simeq (m\epsilon^2 - 2m\epsilon^2)cos(\theta_3 - \theta_2) \leq 0$$

and

$$m\epsilon^2 + ml^2 + I_2 - ml\epsilon cos^2(\theta_3 - \theta_2) \simeq m\epsilon^2 + 4m\epsilon^2 - 2m\epsilon^2cos^2(\theta_3 - \theta_2) \geq 0$$

The above inequalities hold generally, thus looking at (4.16) the claim is easily proven.

The impact theory of the previous section takes care of the discontinuities in velocities when contact is initially achieved. In Wittenburg's analysis this is enough to study the process. Since he deals with perfect rigid bodies with no deformation at all, the impact phenomenon is completed at time $t_0 + \Delta t$ and by using numerical integration he obtains the free motion of the system up to a possible new impact etc. But as was already explained, the deformation of the beam results in a force of finite duration in our case.

In a detailed idealized force profile one could see the plot of Figure 4.3. The initial delta function corresponds to the impulse $\hat{f}$ that was calculated in the previous paragraphs. Its presence is completely theoretical and not much can be done in terms of capturing or controlling it. However, its results (instantaneous velocity increments) that determine the state of the system immediately after initial contact are of great importance.

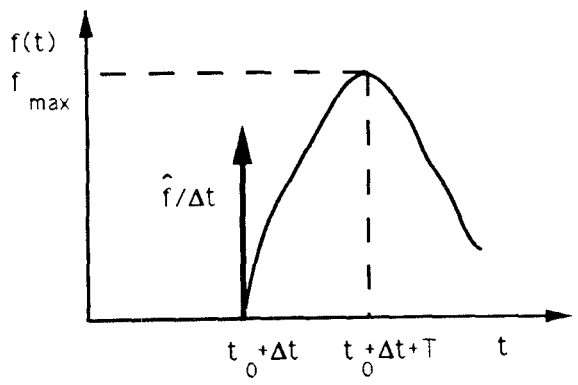

Figure 4.3: Typical contact force profile

It is easy to understand that the smooth motion of the beam just after the initial discontinuity is determined again by the differential equations of motion. In the ideal case where the controller has enough time available, we can solve numerically the problem of predicting the maximum reaction force, using the methodology of the previous chapter. Solving a nonlinear system of equations is generally a time-consuming process for a real-time implementation. A more efficient means must be used in the evaluation of the maximum force on-the-fly. The time delay in this procedure should be a small percentage of the granted sampling period. Some simplifying assumptions are necessary to solve the problem of motion immediately after impact in a comparatively small amount of time.

4.2.1 Some new assumptions

Consider once again the constrained motion of the beam that the numerical methods yielded in the previous chapter. We understand that the delay T between the initial contact and the time where the maximum force is developed, is of the order of milliseconds. For a mechanical system this can be considered a comparatively short amount of time. Therefore, an approximation can be that *velocities have a linear relationship with time for* $t \in [t_0 + \Delta t, t_0 + \Delta t + T]$. Our plots agree with the above assertion. Whether it is acceptable will be judged at the end.

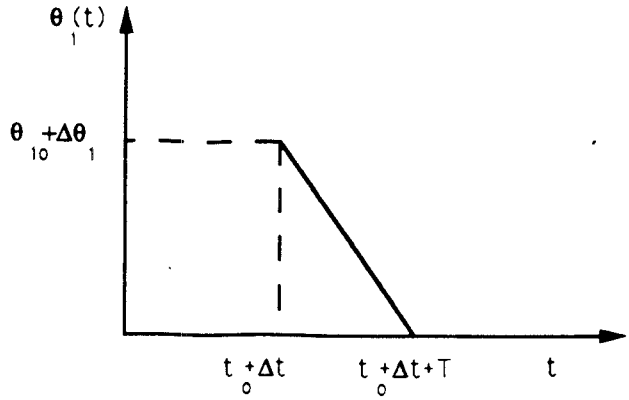

Figure 4.4: Linear approximation of velocity of the ith body for $t \in [t_0 + \Delta t, t_0 + \Delta t + T]$

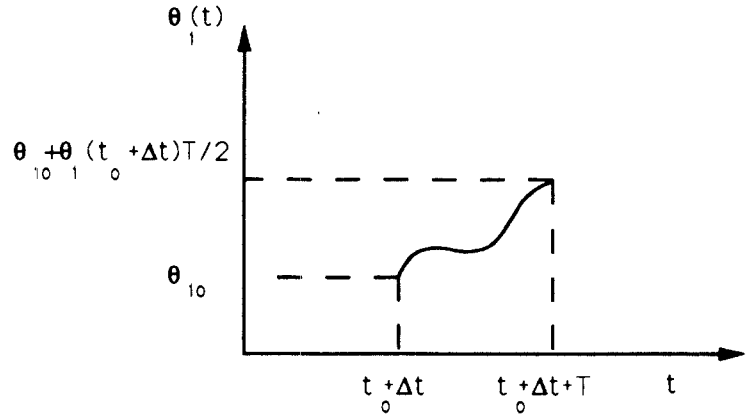

Figure 4.5: Quadratic approximation of displacement of the ith body for $t \in [t_0 + \Delta t, t_0 + \Delta t + T]$

Another important point is that the maximum force corresponds to zero angular velocities for all bodies. Given the above assumptions, a velocity profile of the ith body is shown in Figure 4.4. Then (4.19) holds trivially for $t \in [t_0 + \Delta t, t_0 + \Delta t + T]$

$$\begin{aligned} \theta_i(t) &= \theta_{i0} + \int_{t_0+\Delta t}^{t_0+\Delta t+t} \dot{\theta}_i(\tau)d\tau \\ &= \theta_{i0} + \dot{\theta}_i(t_0 + \Delta t)[(t - t_0 - \Delta t) - \frac{1}{T}\frac{(t - t_0 - \Delta t)^2}{2}]. \end{aligned} \tag{4.19}$$

The corresponding quadratic plot for displacement is presented in Figure 4.5. Now, taking the integral of the differential equations of motion from $t_0 + \Delta t$ up

to $t_0 + \Delta t + T$, where T is finite, we get some similar expressions as in (4.7), (4.8) and (4.9). These give

$$\begin{aligned}\int_{t_0+\Delta t}^{t_0+\Delta t+T} \frac{k_T}{R_a} v(t)dt &= -k_1 \frac{T}{2}[(2\theta_{20} + \frac{T}{2}\dot{\theta}_2(t_0+\Delta t)) - (2\theta_{10} + \frac{T}{2}\dot{\theta}_1(t_0+\Delta t))] \\ &\quad -I_1\dot{\theta}_1(t_0+\Delta t) + [k_{fr} + \frac{k_T k_B}{R_a}]\frac{T}{2}\dot{\theta}_1(t_0+\Delta t) \qquad (4.20)\end{aligned}$$

$$\begin{aligned}0 &= -k_2 T(\theta_{30} - \theta_{20}) - k_2 \frac{T^2}{4}[\dot{\theta}_3(t_0+\Delta t) - \dot{\theta}_2(t_0+\Delta t)] \\ &\quad + k_1 T(\theta_{20} - \theta_{10}) - k_1 \frac{T^2}{4}[\dot{\theta}_2(t_0+\Delta t) - \dot{\theta}_1(t_0+\Delta t)] \\ &\quad + [m_2\epsilon_2^2 + m_3 l^2 + I_2 + m_3 l \epsilon_3 cos(\theta_{30} - \theta_{20})][0 - \dot{\theta}_2(t_0+\Delta t)] \\ &\quad + [m_3\epsilon_3^2 + I_3 + m_3 l \epsilon_3 cos(\theta_{30} - \theta_{20})][0 - \dot{\theta}_3(t_0+\Delta t)] \\ &\quad + \frac{T}{2} l[1 + cos(\theta_{30} - \theta_{20})] f_{max} \qquad (4.21)\end{aligned}$$

$$\begin{aligned}0 &= k_2 T(\theta_{30} - \theta_{20}) + k_2 \frac{T^2}{4}[\dot{\theta}_3(t_0+\Delta t) - \dot{\theta}_2(t_0+\Delta t)] + \frac{T}{2} l f_{max} \\ &\quad - m_3 l \epsilon_3 cos(\theta_{30} - \theta_{20})\dot{\theta}_2(t_0+\Delta t) - [m_3\epsilon_3^2 + I_3]\dot{\theta}_3(t_0+\Delta t). \qquad (4.22)\end{aligned}$$

These three equations have as unknowns the time delay T, the maximum reaction force f_{max} and the velocity $\dot{\theta}_1(t_0 + \Delta t)$. This is a nonlinear system of equations that can be easily solved on-the-fly, using the Newton-Raphson method on a sufficiently fast processor. The results at the end of the chapter were obtained this way.

If time limitations do not allow such a computation, one more approximation can be employed, namely $\Delta\dot{\theta}_1 = \Delta\dot{\theta}_2$. Then

$$\dot{\theta}_1(t_0 + \Delta t) = \dot{\theta}_{10} + \Delta\dot{\theta}_2$$

Here, we end up with a system of the quadratic equations with unknowns T and f_{max}. If this is the case, the effect of the input torque $T_{in}(t)$ on the system for $t \in [t_0 + \Delta t, t_1]$ is neglected.

Remark: It is reasonably assumed that the term $\int_{t_0}^{t_0+\Delta t+T} T_{in}(t)dt$ is given by the following procedure: the controller having used some optimal control method has come up with some optimal $T_{in}(t)$ that minimizes the effect of impact, given the zero terminal velocity constraints and some time restrictions. By the time that T_{in} is prescribed, the above integral is determined.

The results of this method are discussed at the end of the chapter along with the results of the energy principle method.

4.3 Prediction of the maximum reaction force using the energy principle

In recent years, the problem of finding closed form solutions of the maximum impact force has been based exclusively on the energy principle. In most of the cases the problem addressed considers collisions between two single-body systems. Johnson [18] first used the energy principle for the impact force derivation and more recently Amirouche [7] extended the previous method by incorporating the energy loss due to structural damping. It was found that the impact

force equation correlates well with the experimental data but only for low stiffness. Similar results seem to hold in our case as well. This seems to justify the efficiency and the generality of our previous method which works the same over the whole range of stiffness. More comparisons will follow at the end of the section.

This section presents the derivation of the maximum reaction force for the beam collision problem using the energy principle. The method will utilize the kinetic and the potential energy accumulated at the beam. However, we neglect the energy loss due to structural damping of the beam or to air damping (recall the dimensions of the beam may involve substantial air damping). Additionally, we do not take into account the work provided by the motor torque input from $t_0 + \Delta t$ up to $t_0 + \Delta t + T$, since it is comparatively low for such small T. In order not to lose the generality of the method, we will frequently refer to a Galerkin model of N rigid bodies connected by means of torsional springs of known stiffness.

A model representing the beam colliding with the rigid wall was shown in Figure 4.1. This model predicts the overall motion changes from a global viewpoint. The impact collision can be considered equivalent to one half oscillation of this lumped parameter spring-mass system of Figure 4.1. At the start of the collision, the multi-body structure is at state $(\theta_0, \dot{\theta}_0, \ddot{\theta}_0)$, having some kinetic energy KE_0 and some potential energy PE_0 since even in the unconstrained

motion the beam is deformed. By neglecting the energy loss due to air and structural damping as well as the work done by the motor torque input in the time interval T, the total energy just before collision, will start being transformed into strain energy for $t > t_0 + \Delta t$. At the point of maximum deformation (which also corresponds to zero velocities and to maximum force), the system contains just pure potential energy, stored in the torsional springs of the system. If KE_0, PE_0 and PE_{max} denote the total kinetic energy just before contact, the total potential energy just before contact and the total energy (pure potential) at the maximum deformation respectively, then

$$KE_0 + PE_0 = PE_{max}. \tag{4.23}$$

The kinetic energy of each rigid body just before contact is given by the following well-known relations:

$$KE_{10} = \frac{1}{2} I_1 \dot{\theta}_{10}^2$$

$$KE_{20} = \frac{1}{2} I_2 \dot{\theta}_{20}^2 + \frac{1}{2} m_2 \epsilon_2^2 \dot{\theta}_{20}^2$$

$$KE_{30} = \frac{1}{2} I_3 \dot{\theta}_{30}^2 + \frac{1}{2} m_3 \dot{\mathbf{s}}_{\mathbf{30}}^{\mathbf{T}} \dot{\mathbf{s}}_{\mathbf{30}}$$

where $\mathbf{s_3}$ is the position vector of the center of mass of the third body and $\mathbf{s_{30}}$ refers to the configuration immediately before contact.

$$\mathbf{s_3} = [l cos\theta_2 + \epsilon_3 cos\theta_3, l sin\theta_2 + \epsilon_3 sin\theta_3, 0]^T$$

and

$$\dot{\mathbf{s}}_{\mathbf{3}} = [-l sin\theta_2 \dot{\theta}_2 - \epsilon_3 sin\theta_3 \dot{\theta}_3, l cos\theta_2 \dot{\theta}_2 + \epsilon_3 cos\theta_3 \dot{\theta}_3, 0]^T$$

therefore,

$$KE_{30} = \frac{1}{2}m_3[l^2\dot{\theta}_{20}^2 + \epsilon_3^2\dot{\theta}_{30}^2 + 2l\epsilon_3\dot{\theta}_{20}\dot{\theta}_{30}cos(\theta_{30} - \theta_{20})].$$

The mechanical system just before contact has potential energy which is given by

$$PE_0 = \frac{1}{2}k_1(\theta_{20} - \theta_{10})^2 + \frac{1}{2}k_2(\theta_{30} - \theta_{20})^2.$$

Energy Quasi-Principle: In the general case where we have a model of n springs of known stiffness connected in series, we postulate that the following holds for the ith spring

$$\frac{PE_{i,max}}{PE_{max}} = \frac{(1/k_i)}{\sum_{j=1}^{n}(1/k_j)} \tag{4.24}$$

where $(PE_{i,max}/PE_{max})$ is the percentage of the potential energy that the ith element receives at the maximum deformation configuration. □

A partial justification for this principle may be derived from electrical circuit theoretic analogies. We omit the details. A more rigorous justification of the statement requires further study[2].

In our case, the total energy $(\sum_{i=1}^{3} KE_{i0} + PE_0)$ will be distributed as strain energy on the springs k_1 and k_2 in a predicted manner according to (4.24). The above are summarized in the next two relationships

$$\frac{1}{2}k_1(\theta_{2,max} - \theta_{1,max})^2 = \frac{k_2}{k_1 + k_2}(PE_0 + \sum_{i=1}^{n} KE_{i0}), \tag{4.25}$$

[2]The above quasi-principle assumes that the maximum deformation configuration corresponds to zero velocities for all rigid bodies of the system (stationary point). However, there might be cases where this is not generally true.

$$\frac{1}{2}k_2(\theta_{3,max} - \theta_{2,max})^2 = \frac{k_1}{k_1 + k_2}(PE_0 + \sum_{i=1}^{n} KE_{i0}) \tag{4.26}$$

Equations of this type for N-body problems specify angle differences of the form $(\theta_{i+1,max} - \theta_{i,max})$. For our purposes, this is sufficient to determine the maximum deformation configuration of the beam (in terms of position), since the energy principle does not involve absolute displacements[3].

At the state of maximum deformation (i.e. maximum force) configuration we also expect velocities to become zero. Accelerations are generally non-zero but there is no need of determining them. Given the above observations, the dynamic equations of motion under the steady state of maximum deformation become:

$$\frac{k_T}{R_a}v(t_0 + \Delta t + T) = I_1\ddot{\theta}_1(t_0 + \Delta t + T) - k_1(\theta_{2,max} - \theta_{1,max}) \tag{4.27}$$

$$\begin{aligned} 0 \;=\; & -k_2(\theta_{3,max} - \theta_{2,max}) + k_1[\theta_2(t_0 + \Delta t + T) - \theta_1(t_0 + \Delta t + T)] \\ & +[m_2\epsilon_2^2 + m_3l^2 + I_2 + m_3l\epsilon_3cos(\theta_{3,max} - \theta_{2,max})]\ddot{\theta}_2(t_0 + \Delta t + T) \\ & +[m_3\epsilon_3^2 + I_3 + m_3le_3cos(\theta_{3,max} - \theta_{2,max})]\ddot{\theta}_3(t_0 + \Delta t + T) \\ & +f_{max}l[1 + cos(\theta_{3,max} - \theta_{2,max})] \end{aligned} \tag{4.28}$$

$$\begin{aligned} -k_2(\theta_{3,max} - \theta_{2,max}) \;=\; & m_3l\epsilon_3cos(\theta_{3,max} - \theta_{2,max})\ddot{\theta}_2(t_0 + \Delta t + T)) \\ & +[m_3\epsilon_3^2 + I_3]\ddot{\theta}_3(t_0 + \Delta t + T) + f_{max}l \end{aligned} \tag{4.29}$$

[3]In the next paragraphs we should observe that all displacement terms present in the dynamic equations and in the kinematic constraint are of the form $(\theta_{i+1,max} - \theta_{i,max})$.

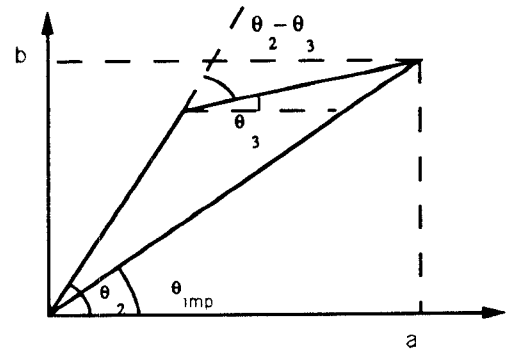

Figure 4.6: Configuration of the beam model at maximum deformation

Apparently, we need one more equation to solve for the accelerations and the force at the time instant $(t_0 + \Delta t + T)$. Notice once again, that the first equation is decoupled from the rest and it is unimportant. The additional equation comes from the kinematic constraint (3.13):

$$\begin{aligned} 0 &= [acos\theta_{3,max} + bsin\theta_{3,max} - lcos(\theta_{3,max} - \theta_{2,max})]\ddot{\theta}_3(t_0 + \Delta t + T) \\ &\quad + lcos(\theta_{3,max} - \theta_{2,max})\ddot{\theta}_2(t_0 + \Delta t + T) \end{aligned} \tag{4.30}$$

In the above equation only known angle differences are present except for the term $(acos\theta_{3,max} + bsin\theta_{3,max})$. This can be also written as a function of angle differences as such (see Figure 4.6):

$$acos\theta_{3,max} + bsin\theta_{3,max} = 2lcos(\theta_{2,max} - \theta_{imp})cos(\theta_{3,max} - \theta_{imp})$$

By the geometry of the problem,

$$\theta_{3,max} = \theta_{imp} + \frac{\theta_{3,max} - \theta_{2,max}}{2} \tag{4.31}$$

$$\theta_{2,max} = \theta_{imp} - \frac{\theta_{3,max} - \theta_{2,max}}{2}. \tag{4.32}$$

Hence,

$$\begin{aligned} acos\theta_{3,max} + bsin\theta_{3,max} &= 2lcos(-\frac{\theta_{3,max} - \theta_{2,max}}{2})cos(\frac{\theta_{3,max} - \theta_{2,max}}{2}) = \\ &= 2lcos^2(\frac{\theta_{3,max} - \theta_{2,max}}{2}) = \\ &= l[1 + cos(\theta_{3,max} - \theta_{2,max})]. \end{aligned} \tag{4.33}$$

Therefore, (4.30) becomes

$$lcos(\theta_{3,max} - \theta_{2,max})\ddot{\theta}_2(t_0 + \Delta t + T) + l\ddot{\theta}_3(t_0 + \Delta t + T) = 0. \tag{4.34}$$

Equations (4.28), (4.29) and (4.34) can now be used to evaluate the maximum reaction force f_{max}. Notice that the complexity of the problem is lower than that of the previous method, since only one matrix inversion is involved here. However, there is no means provided for determining the delay T between contact time and time of maximum force development. The results of this method follow in the next sections.

Some remarks about structural damping: The above method can be apparently improved by including the structural damping of the beam or/and the air damping. As far as the structural damping is concerned, this is due to natural causes inherent to the mechanical system (material damping, internal friction, internal damping or hysteretic damping). In solids, the nature of the internal forces which produce dissipative effects is generally very complex and varies considerably between different types of materials.

For the continuum equations of elasticity, some dissipative mechanisms such

as square root damping and rate damping can be incorporated in the modeling (a more detailed analysis can be found in [17]). For single degree of freedom systems as in Figure 4.1 , the types of damping encountered are viscous and hysteretic (linear) as well as Coulomb damping (nonlinear). Unfortunately, the absolute energy dissipation due to structural damping for some given material and dimensions, is not easily determined empirically with sufficient precision. This amount of energy loss may be negligible. Nevertheless, *the structural damping does lower the maximum reaction force during collision.*

4.4 Comparison of the two methods for evaluating the maximum reaction force

The results of the above methods for evaluating the maximum reaction force are presented and discussed here. The comparisons use as reference the detailed numerical analysis of Chapter 3 which we accept as valid. Each table refers to a specific stiffness of the beam. As was mentioned before, all recent work on impact between single-body systems that used the energy principle based method, failed to match well with the experimental results for high spring constants. The first method using impact dynamics seemed to be unaffected over the whole range of beam stiffness and this is an important advantage in terms of its generality.

For stiffness of the beam $100 \times$ *nominal value*, the maximum reaction force

	1.0V	2.0V	5.0V	10.0V
max force by energy principle in N	23.93	35.87	58.41	82.92
max force by impact dynamics in N	17.92	27.36	46.12	67.76
actual force by detailed simulation in N	17.44	26.63	44.28	65.36
time delay by impact dynamics in sec	0.005	0.005	0.006	0.006
time delay by simulation in sec	0.005	0.005	0.005	0.005

Table 4.1: Prediction results for $k_2 = 100 \times nominal\ value$

	1.0V	2.0V	5.0V	10.0V
max force by energy principle in N	7.26	10.79	17.32	23.56
max force by impact dynamics in N	5.82	9.18	16.46	23.23
actual force by detailed simulation in N	5.63	8.72	14.73	22.75
time delay by impact dynamics in sec	0.018	0.019	0.018	0.020
time delay by simulation in sec	0.016	0.015	0.015	0.015

Table 4.2: Prediction results for $k_2 = 10 \times nominal\ value$

as well as the delay time derived by the impact dynamics method, were very close to those of the detailed numerical analysis. Recall that this was expected, since the assumption of linear approximation for, velocities and displacements is more valid as the duration of the impact shrinks. The tendency of the energy principle method to give higher force values for the same stiffness, is because the structural damping was neglected.

In the intermediate case where $k_2 = 10 \times nominal\ value$, the energy principle starts giving acceptable results, but still the absence of damping apparently affects the method. As the stiffness value is decreased to its nominal value, the same method gives smaller values for the impact force which might confound the controller. An explanation is that the damping effect is less severe, but since

	$1.0V$	$2.0V$	$5.0V$	$10.0V$
max force by energy principle in N	2.04	2.95	4.72	4.73
max force by impact dynamics in N	2.05	3.45	6.89	8.57
actual force by detailed simulation in N	1.84	2.95	5.22	7.43
time delay by impact dynamics in sec	0.062	0.063	0.060	0.109
time delay by simulation in sec	0.048	0.047	0.044	0.033

Table 4.3: Prediction results for $k_2 = nominal\ value$

the duration of the pulse is enlarged, the work provided by the motor input torque becomes more substantial. For the nominal k_2, although the impact dynamics method could not provide an outstanding response for the delay time, it still provides good results for the f_{max}. It is perhaps worth noticing that for a sampling frequency of $100Hz$ and for nominal stiffness, the maximum and the minimum delays T are just one sampling period far away. The controller already knows in advance that it has at the most 4 sampling periods to respond in order to diminish the effect of impact, whatever the maximum force happens to be. Therefore, the accuracy of the time delay T is of less importance. As far as complexity is concerned, the energy principle method is much simpler since it involves just a matrix inversion, while the impact dynamics method requires the solution of a comparatively simple nonlinear system of equations.

Since the next thing that one has in mind after all this analysis, is the design of the *impact controller*, let us give here the most important advantage of the impact dynamics method: the energy principle method is just capable of providing an indication *on-the-fly* of how aggressive the impact phenomenon will

be in the case of collision and therefore can advice the controller to reduce the current velocity if a threshold was exceeded. But since the method does not take into account the term $\int_{t_0+\Delta t}^{t_0+\Delta t+T} v(\tau)d\tau$ it is not of much help to the controller in determining the optimal control input $v(t)$. It is the impact dynamics method that can provide answers to trial and error type questions that may arise during the investigation of the optimal control.

The results of this section serve as a justification for the amount of effort spent to understand the detailed dynamics of the impact problem. The energy methods used in the past for the maximum force prediction, are not precise enough to be used for controlling impact of multi-body structures.

Chapter 5

Real-time implementation of an impact-force control law

5.1 Historical perspective of impact control

As was mentioned earlier, two methods are commonly used to control the impact overshoot, depending on the availability of the object position in advance:

1. Given the position of the object in advance (through some kind of sensory feedback), control the impending contact velocity just prior to impact.

2. Approach the workpiece with some constant velocity, while monitoring the sensed force for contact. As soon as contact is detected, the force controller is turned on. This method assumes that no information about the object position is available.

In case (1) the contact velocity is controlled, assuming that the necessary positioning information is available. Optimal control theory provides an analysis methodology for addressing the minimal time problem subject to the zero terminal velocity constraint, in the case of rigid manipulators. The results of this technique suggest us to drive the system with maximum positive control effort until some time T^*, at which time the maximum negative control effort is applied. Such control has been conventionally labeled *bang-bang* control. The terminal velocity will be zero and no impact will take place if the switching time T^* is properly chosen. The switching time T^* depends on the object shape, geometry and location. Object misalignment or robot positioning inaccuracies might affect the control severely. Thus the sensory feedback on object proximity is absolutely necessary to determine T^* on-the-fly. Matters get more complicated in the case of flexible manipulators where inertia and flexibility count for negative initial acceleration at the end-effector. Some simple experiments on our flexible beam for example, proved that bang-bang control actually results in greater reaction forces and deteriorates the impact problem. Therefore, more sophisticated control algorithms must be employed which should include the dynamics of the bodies involved.

The rest of the discussion refers to the more realistic case (2), where the impact controller obtains no positioning information in advance. In most of the relevant previous research, the impact phenomenon was treated by the same controller that was used to follow a commanded force. Only in recent years,

methods were suggested to diminish the impact transient by tuning the force controller gains for the best impact response. To the best of the author's knowledge, Youcef-Toumi and D. Gutz [27] were the first to investigate the problem of impact in robotic manipulators in an experimentally based methodology. The experiments carried out by the above-mentioned researchers, were performed on a one degree-of-freedom dynamically decoupled arm, in a set-up very similar to our flexible beam. Some immediate conclusions of their work are listed below:

1. The allowed approach speed is directly proportional to the desired contact force level.

2. With a softer environment and/or sensor, the gain of the controller can be larger and consequently a faster movement of the arm is allowed[1].

3. Integral explicit force control acts as a low-pass filter; thus this type of control filters effectively the high frequency components of the impact transient and it is well suited for force tracking as well.

Other authors have addressed the problem of controlling manipulators subject to impulsive forces. A discontinuous control algorithm that results in a system that is stable during both noncontact and contact modes, was proposed by Mills [9]. Mills in his analysis assumes exact knowledge of the system parameters and the contact force and models the environment as a surface of

[1]Actually, deliberate compliance in the combined workpiece-sensor -arm dynamics is so far, the only solution consistent with fast response and low contact forces.

finite stiffness and damping. Using a two degrees-of-freedom, five bar parallel link configuration operating in the horizontal plane, he claimed that the closed loop system response is ultimately bounded for transitions from noncontact to contact motion.

Open loop design schemes were proposed as well, since feedback tends to obscure the impact effect (because of inability of force transducers to respond in high frequency excitations). The computed torque method proposed by Bayo [2] uses a Fast Fourier Transform applied to the global equations of motion. The method, originally presented for position control of open-chain flexible robots, was well-adapted for force control. It may be considered as an extension of the Newton-Euler formulation for the inverse dynamics.

S.Eppinger and W.Seering [20] investigated the dynamic modeling of robot force control. Active force control systems that have been implemented, demonstrated stability problems. Instabilities can be caused by link flexibility, actuator bandwidth, digital sampling rate, backlash, bearing friction etc. They proved that *instability is present when the sensor is located at a point remote from the actuator (noncollocation effect).* The controller in this case attempts to regulate the contact force through a dynamical system. Given that, many researchers have been skeptical about deliberate link flexibility and proposed that *every element between each actuator-sensor pair should be designed with high stiffness in mind.* If this cannot be avoided (all robots have some degree of flexibility), use

of flexible structures in the view of these researchers, requires either an exact system model or the use of an auxiliary collocated sensor.

Finally, we should include in the literature review the naive method of preventing the impact effect by limiting the impending contact velocity under a certain threshold. For a robotic arm with flexibility, however, this threshold which obviously corresponds to the worst contact case, might be very restrictive. An explanation of the above assertion is that *a certain tip velocity can cause different maximum impact forces at different given states of beam motion.* If the tip position follows an oscillatory- type trajectory while on free motion, it really helps to know if initial contact is made in-phase or not. In particular, one should consider the possibility that the beam achieves contact while the tip has a negative acceleration. Therefore, the velocity threshold is a function of time, probably of sinusoidal form. The minimum of this threshold function with respect to time should be picked, which apparently results in a sluggish movement of the flexible arm.

Having discussed the previous schemes for impact control and their weaknesses, we proceed in the next sections with a newly proposed strategy. The corresponding analysis will provide justification to the simplified model used and to the control algorithm.

5.2 The simplified model

The equations of motion of the beam (2.15),(2.16) and (2.17) may be restated in a more general form

$$\mathbf{M}(\theta)\ddot{\theta} + \mathbf{C}(\theta, \dot{\theta}) + \mathbf{K}(\theta) = \mathbf{u} - \mathbf{f} \tag{5.1}$$

where $\mathbf{M}$ and $\mathbf{K}$ are the conventional finite element mass and stiffness matrices respectively; $\mathbf{C}$ includes the nonlinear Coriolis, centrifugal and motor damping-stiction terms. The vector $\mathbf{u}$ contains one non-zero term only, in the first entry, and that is the torque at the hub. $\mathbf{f}$ contains the unknown reaction forces at each body.

In order to describe the constrained motion of the beam, we should include the kinematic constraint equation. Let us consider the general case of the N-body Galerkin approximation. By expanding the trigonometric terms of the kinematic constraint into Taylor series (see equation (3.9) for the 2nd order approximation) and keeping the first order terms of the expansion , one can get the simplified kinematic constraint of the N-body problem:

$$\sum_{k=1}^{N} \theta_k = N\theta_{imp} \tag{5.2}$$

where θ_{imp} is the impact angle determined at the tip. Since the above relation is a natural holonomic constraint, its derivatives can be included in our model

as well, whenever contact exists:

$$\sum_{k=1}^{N} \dot{\theta}_k = 0 \tag{5.3}$$

$$\sum_{k=1}^{N} \ddot{\theta}_k = 0 \tag{5.4}$$

which actually correspond to equations (3.12) and (3.13). It is clear that we have $N+1$ dynamic equations (the additional one reffers to the hub body), plus the natural constraints (5.2),(5.3) and (5.4). However , we have $3(N+1)+1$ unknowns, namely the accelerations, velocities and the displacements of all bodies, plus the normal reaction force at the tip. Therefore, in order to solve the control problem, we are forced to use a low order finite element approximation for the beam. The explanation is that we are unable to measure the additional states of an N-order model. *Observers that usually work for position control of flexible structures, seem to be worthless here, since the short settling time that is required for tracking the impact effect, may result in high observer gains and instability.* Even in the case of a fast analog observer, same additional delays will be involved in translating the position information of the shaft-encoders into analog format. For the time being, only velocity and angular displacement of the shaft are measurable, while the FSR is capable of detecting contact in a zero-one mode. Its performance is limited to capturing low-frequency events. Other type of force transducers should be used to close the feedback loop for impact control (e.g. piezoelectric type), although their performance may depend again on the computing power available and the interface delays.

Given the above considerations, we proceed with a 2nd order model, justified by the insufficient state measurements. Additionally, we will assume that the hub and the beam are rigidly coupled ($k_1 = \infty$), so that the position encoder measures the angle $\theta_2 = \theta_1$ of the first rigid body of the beam approximation. Finally, we assume that the impact angle θ_{imp} is given in advance, just for the purpose of evaluating the angle θ_3 *on-the-fly* through the kinematic constraint equation (5.2).

Note: The above assumption does not mean that we know the object position in advance. We use this information only when contact is already established. This is not the only way to proceed. We shall see that instead of giving the impact angle, we can alternatively measure the tip force or the acceleration at the hub. Since none of these measurements is available at this time, the knowledge of impact angle was considered necessary.

The dynamic model of the 2nd order approximation along with the natural constraints are summarized below:

$$\frac{k_T}{R_a}v(t) = I_1\ddot{\theta}_1 - k_1(\theta_2 - \theta_1) + k_{fr}\dot{\theta}_1 + k_{st}sgn(\dot{\theta}_1) + \frac{k_T k_B}{R_a}\dot{\theta}_1 \tag{5.5}$$

$$\begin{aligned} k_2(\theta_3 - \theta_2) - k_1(\theta_2 - \theta_1) &= [m_2\epsilon_2^2 + m_3 l^2 + I_2 + m_3 l\epsilon_3 cos(\theta_3 - \theta_2)]\ddot{\theta}_2 \\ &\quad +[m_3\epsilon_3^2 + I_3 + m_3 l\epsilon_3 cos(\theta_3 - \theta_2)]\ddot{\theta}_3 \\ &\quad -m_3 l\epsilon_3 sin(\theta_3 - \theta_2)(\dot{\theta}_3^2 - \dot{\theta}_2^2) \\ &\quad +fl[1 + cos(\theta_3 - \theta_2)] \end{aligned} \tag{5.6}$$

$$
\begin{aligned}
-k_2(\theta_3-\theta_2) &= m_3 l\epsilon_3 cos(\theta_3-\theta_2)\ddot{\theta}_2 + [m_3\epsilon_3^2 + I_3]\ddot{\theta}_3 \\
&\quad + m_3 l\epsilon_3 sin(\theta_3-\theta_2)\dot{\theta}_2^2 + fl \qquad (5.7)
\end{aligned}
$$

$$
\theta_2 + \theta_3 = 2\theta_{imp} \qquad (5.8)
$$

$$
\dot{\theta}_2 + \dot{\theta}_3 = 0 \qquad (5.9)
$$

$$
\ddot{\theta}_2 + \ddot{\theta}_3 = 0 \qquad (5.10)
$$

Using the constraint equations (5.8), (5.9) and (5.10), and making the approximation $cos(\theta_3-\theta_2) \approx 1$, we can get a simplified model of the constrained motion. Actually, for the given stiffness of the beam and for the maximum deformation which corresponds to the maximum output motor torque, the above cosine can be found to be 0.995.

$$
\frac{k_T}{R_a}u(t) = k_{fr}\dot{\theta}_2 + k_{st}sgn(\dot{\theta}_2) + \frac{k_T k_B}{R_a}\dot{\theta}_2 - k_2(\theta_3-\theta_2) + 4m\epsilon^2\ddot{\theta}_2 + 2fl \qquad (5.11)
$$

$$
-k_2(\theta_3-\theta_2) = m\epsilon^2\ddot{\theta}_2 + fl \qquad (5.12)
$$

The above equations comprise a simplified model, where θ_2 and $\dot{\theta}_2$ are measurable, while f, $\ddot{\theta}_2$ and θ_3 are unknown. In order to evaluate the complete state of our model, we can either measure $\ddot{\theta}_2$ or f or we can give θ_{imp} in advance. By eliminating the reaction force from the above equations and knowing the impact angle , we get

$$
\frac{k_T}{R_a}u(t) = k_{fr}\dot{\theta}_2 + k_{st}sgn(\dot{\theta}_2) + \frac{k_T k_B}{R_a}\dot{\theta}_2 - 6k_2(\theta_{imp}-\theta_2) + 2m\epsilon^2\ddot{\theta}_2 \qquad (5.13)
$$

The above equation will be the simplified model of the constrained motion of the beam. Bear in mind that this model holds *only when contact exists.* The reaction force is not explicitly present since it was eliminated using the constraint equations. Just for comparison purposes, we derive a closed form expression for the tip force using (5.12) above:

$$f = -\frac{2K_2}{l}(\theta_{imp} - \theta_2) - \frac{m\epsilon^2}{l}\ddot{\theta}_2 \tag{5.14}$$

This equation gives a theoretical approximation of the reaction force, which complements the noisy FSR output.

5.3 The proposed impact-force control strategy

The impact-force controller should complete the following task:

- approach the workpiece (rigid wall) by applying a constant input voltage to the actuator.

- as soon as contact is established, apply some desired force on the workpiece.

The design criteria should be *small force overshoot, fast settling time and bouncing avoidance* (i.e. establish contact once and for all). Three clear states are identified in this interaction with the environment: (i) motion in free space, (ii) constrained motion - impact and (iii) constrained motion - contact. For these type of operations we propose the following control scheme:

1. the controller monitors contact through the FSR output, while in free space.

2. when contact is detected, we specify the open loop displacement, velocity and acceleration trajectories that the system should follow, using the simplified dynamic model of the previous section; we close the loop by penalizing deviations from the desired displacement and velocity profiles.

3. once the transient phenomenon is over and contact is established, the force regulator is turned on (PD control), making the last minor corrections.

The functions of each controller mode as well as the switching criteria are discussed in detail in the following paragraphs.

The first controller mode is just a naive version of position control. For the time being, no care is devoted to keep the impending contact velocity within appropriate limits. By appropriate limits we mean not exceeding some initial contact velocity threshold that may result in instability or inability-to-respond of the impact - force controller. However, the theory behind this story is already developed. Equations (4.20), (4.21) and (4.22) determine the maximum impact force that will be present at the tip if contact is achieved in the very next time step, given some voltage input $u(t)$. If the force threshold is exceeded then a correcting input voltage should be applied while still in free space.

In parallel, the controller monitors the reaction force at the tip through the

FSR. When contact is detected the controller switches to the impact mode. At this point we should keep in mind that the force sensor output of the most common transducers (piezoelectric, FSR, strain-gauge), goes off-scale during the short impact interaction, although these sensors may have exceptional rise delays. Therefore, explicit force feedback terms cannot exclusively determine the impact control actions. Open-loop type control was employed instead, based on the inverse dynamics. The algorithm was borrowed from the well known theory of position control[2] and can be found in [14]. Suppose that contact is initially detected at time t_0. At this time the beam is at some arbitrary state $(\theta, \dot{\theta}, \ddot{\theta})$. We wish to attain some new state $(\theta_d, \dot{\theta}_d, \ddot{\theta}_d)$ at time t_f. One way to generate a smooth curve is by using a polynomial function of t. Since we have three initial and three terminal constraints for $\theta_2, \dot{\theta}_2$ and $\ddot{\theta}_2$, we require a polynomial with six independent coefficients that may be chosen to satisfy these constraints. Thus, we consider a 5th order polynomial of the form

$$\theta_2(t) = a_5 t^5 + a_4 t^4 + a_3 t^3 + a_2 t^2 + a_1 t + a_0. \tag{5.15}$$

Then the desired velocity and acceleration are automatically given as

$$\dot{\theta}_2(t) = 5a_5 t^4 + 4a_4 t^3 + 3a_3 t^2 + 2a_2 t + a_1, \tag{5.16}$$

$$\ddot{\theta}_2(t) = 20a_5 t^3 + 12a_4 t^2 + 6a_3 t + 2a_2. \tag{5.17}$$

Without loss of generality, we can set $t_0 = 0$. Then from the initial conditions

[2]Recall that force control can be considered delicate position control, especially in the case of flexible manipulators.

we can easily get the following

$$a_0 = \theta_{20}, \quad a_1 = \dot{\theta}_{20}, \quad 2a_2 = \ddot{\theta}_{20}$$

From the terminal conditions we similarly get

$$\theta_{2f} = a_5 t_f^5 + a_4 t_f^4 + a_3 t_f^3 + a_2 t_f^2 + a_1 t_f + a_0 \tag{5.18}$$

$$\dot{\theta}_{2f} = 5a_5 t_f^4 + 4a_4 t_f^3 + 3a_3 t_f^2 + 2a_2 t_f + a_1 \tag{5.19}$$

$$\ddot{\theta}_{2f} = 20a_5 t_f^3 + 12a_4 t_f^2 + 6a_3 t_f + 2a_2 \tag{5.20}$$

Given the assumptions of the previous subsection, the initial state $(\theta_{20}, \dot{\theta}_{20}, \ddot{\theta}_{20})$ is completely defined, since θ_{20} and $\dot{\theta}_{20}$ are measured on-line, while the unknown $\ddot{\theta}_{20}$ can be easily evaluated from equation (5.13) as soon as contact is detected

$$\frac{k_T}{R_a} u_0 = k_{fr}\dot{\theta}_{20} + k_{st} sgn(\dot{\theta}_{20}) + \frac{k_T k_B}{R_a}\dot{\theta}_{20} - 6k_2(\theta_{imp} - \theta_{20}) + 2m\epsilon^2\ddot{\theta}_{20} \tag{5.21}$$

About the terminal conditions of the beam, consider the steady-state mode. In this case obviously all velocities and accelerations become zero.

$$\frac{k_T}{R_a} u_f = -6k_2(\theta_{imp} - \theta_{2f}) \Rightarrow u_f = \frac{3f_f l}{(k_T/R_a)} \tag{5.22}$$

$$-2k_2(\theta_{imp} - \theta_{2f}) = f_f l \Rightarrow \theta_{2f} = \theta_{imp} + \frac{f_f l}{2k_2} \tag{5.23}$$

where f_f is the desired reaction force at the tip (this is the actual input to the controller). Now, the unknown coefficients can be found by solving the 3rd order linear system of equations (5.18), (5.19) and (5.20). However, this pure open loop control scheme is always subject to external disturbances (recall that the dynamic model is greatly simplified). One improvement might be to close the

loop by penalizing deviations from the desired displacement and velocity profiles since such dependable feedback exists. The closed loop gains are chosen by trial and error (some indications were found in [23]) and they aré identical to the ones used in the force controller. The impact control law is summarized in (5.24),

$$\begin{aligned}\frac{k_T}{R_a}u &= (k_{fr} + \frac{k_T k_B}{R_a})\dot{\theta}_{2d} + k_{st} sgn(\dot{\theta}_{2d}) - 6k_2(\theta_{imp} - \theta_{2d}) + 2m\epsilon^2\ddot{\theta}_{2d} \\ &+ k_p(\theta_{2d} - \theta_2) + k_v(\dot{\theta}_{2d} - \dot{\theta}_2). \end{aligned} \tag{5.24}$$

After the application of the open loop impact control for t_f seconds, the state of the system is close or it should be close to the desired one. It is an easy job for a simple PD-type control law to make the last corrections. The closed loop gains were empirically chosen, while the constant terminal input voltage u_f was evaluated using (5.14) since no dependable force feedback exists[3]:

$$\begin{aligned} u(t) &= k_p(\theta_{2d} - \theta_2) + k_v(\dot{\theta}_{2d} - \dot{\theta}_2) + u_f \\ &= k_p(\theta_{imp} + \frac{f_f l}{2k_2} - \theta_2) + k_v(0 - \dot{\theta}_2) + \frac{3f_f l}{(k_T/R_a)} \end{aligned} \tag{5.25}$$

where $k_p = 10.15$ and $k_v = 0.75$.

It is worth noting that no restriction applies on the switching time t_f from the impact control mode to the force control mode. In the current design t_f was chosen by trial and error under the criterion of smooth transition between modes. Roughly speaking, small t_f is allowed for small contact velocities, while bigger one should be picked in the case of aggressive impact events, where the

[3]Commanded force is translated into desired position

impact controller is assigned to dissipate higher collision energy amounts. The theoretical justification of the optimal switching time is still an open subject.

5.4 Real-time implementation

The real-time control task is performed by an IBM-AT under a sampling frequency of 200Hz. Lower frequencies proven to be insufficient for controlling such short events as impact. The controller uses the simplified model of section 5.2 from the time of initial contact and thereafter. However, this is not generally acceptable, since *the simplified model holds only when contact is established.* The ideal controller should accommodate loss of contact (and consequently handle more aggressive impact effects) by switching from impact control back to some type of position control when contact is lost. For the stated sampling frequency, the computing power of the AT is quite limited, making such tasks infeasible to achieve. Obviously, the performance of the implemented controller is considerably degraded when loss of contact cannot be prevented.

The real-time implementation involves accurate knowledge of the model constants. Given that no dependable analog force feedback exists, one should be very cautious about the correct value of beam stiffness in order to translate tip forces into corresponding beam deviations (body angles). Since stiffness k_2 is not constant but it varies non-linearly with the applied torque, a look-up table was

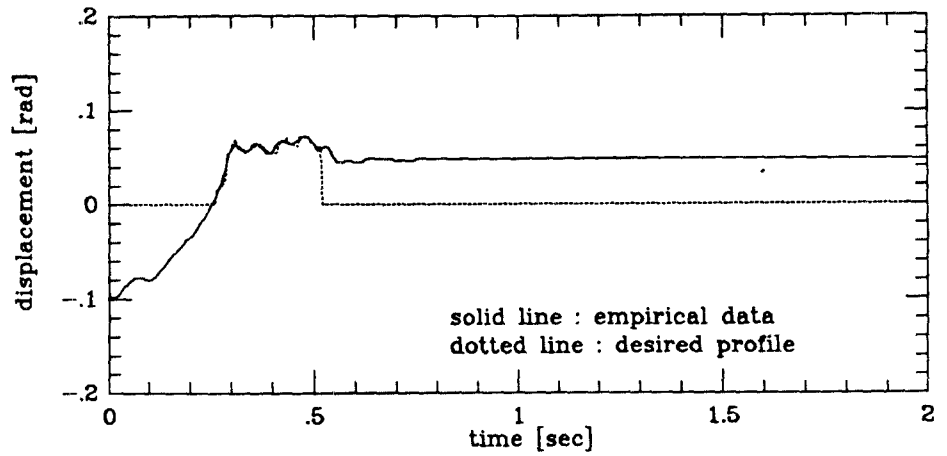

Figure 5.1: Position encoder output for impact response and desired position profile

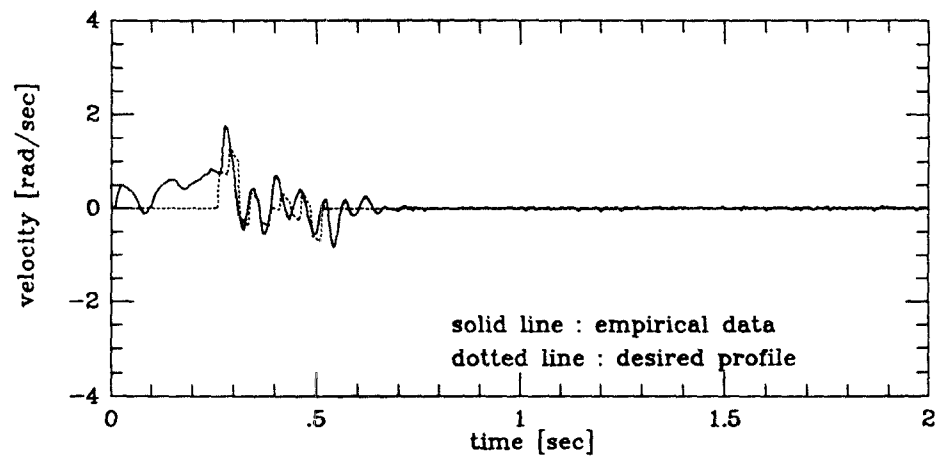

Figure 5.2: Tachometer output for impact response and desired velocity profile

developed in advance. The input to this table is the steady-state force that we desire to apply (a nice way to evaluate the stiffness of the beam experimentally).

$$\theta_{2f} = \theta_{imp} + \frac{f_f l}{2K_2} \Rightarrow K_2 = \frac{f_f l}{2(\theta_{2f} - \theta_{imp})} \tag{5.26}$$

We keep nominal values for all other parameters, presented in Chapter 1. Figures 5.1 and 5.2 show the empirical impact response received by the position

encoder and the tachometer respectively along with the desired position and velocity profiles of the impact mode. The current data hold for impact angle $0rad$ and for initial input voltage $1.0V$. The beam is excited while it is at rest in an arbitrary, negative position. We can easily observe that the desired position profiles are closely followed during the impact control phase (the difference between the experimental data and the desired profiles after $t \simeq 0.5sec$ is because the force controller is turned on). This is not the case for the velocity profiles. Instability problems arising from the abrupt instantaneous velocity increments, do not allow high derivative feedback gains in the impact controller loop.

Figure 5.3 presents the noisy FSR output for the tip reaction force, which is complemented by Figure 5.4 of the theoretical tip force as calculated by equation (5.14). Figure 5.5 shows the control signal to the motor. The total impact phenomenon lasts around $300msec$, however, acceptable force level is applied after $100msec$. The duration of the impact control law is commanded to be $350msec$.

The performance of the controller approaches non-impact performance as the desired steady-state force increases. Higher desired force is generally helpful (below the point of oscillatory behavior), since in the case that the beam bounces, the commanded force acts to restore contact. Figures 5.6 and 5.7 present the corresponding results for such a case. Clearly, the impact effect lasts around $100msec$.

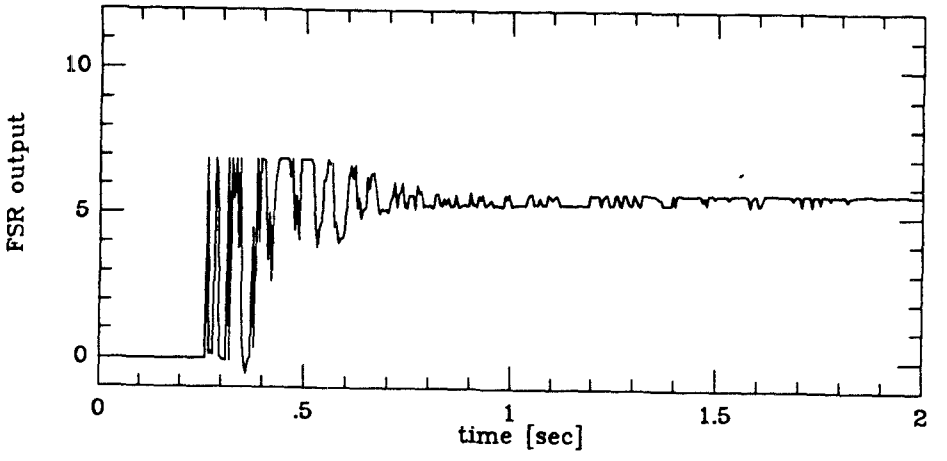

Figure 5.3: Force transducer output for impact response

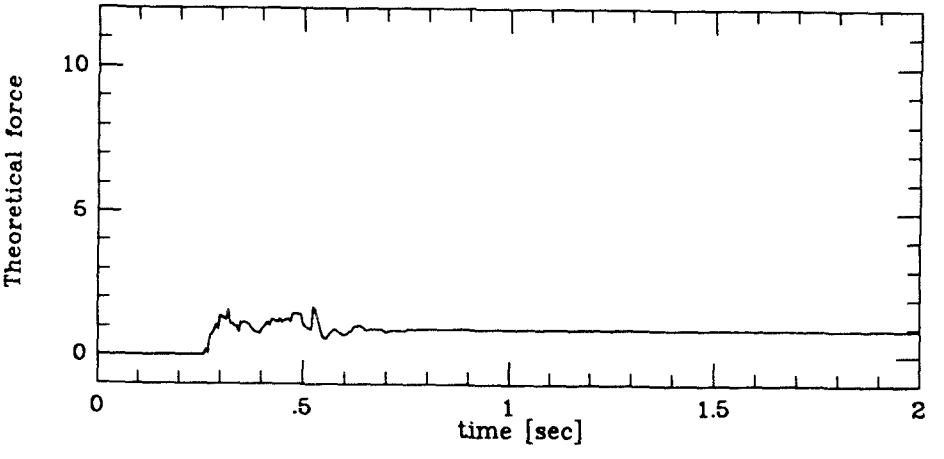

Figure 5.4: Calculated tip force for impact response

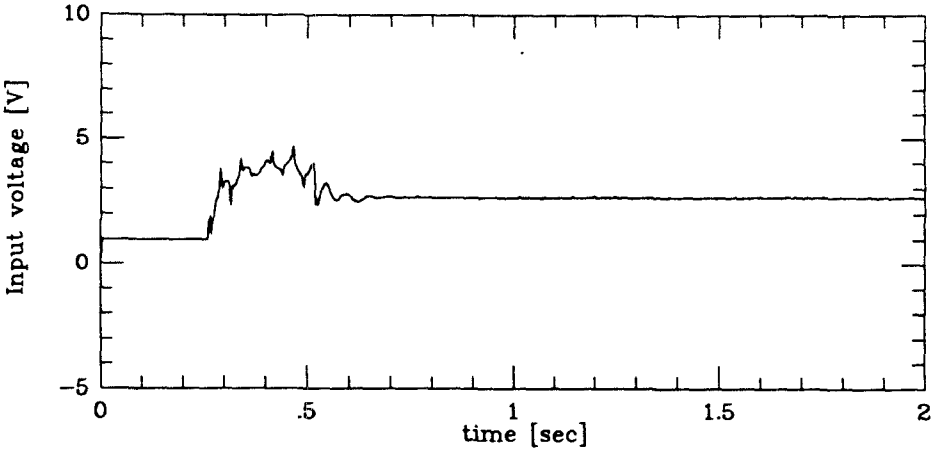

Figure 5.5: Control signal to motor

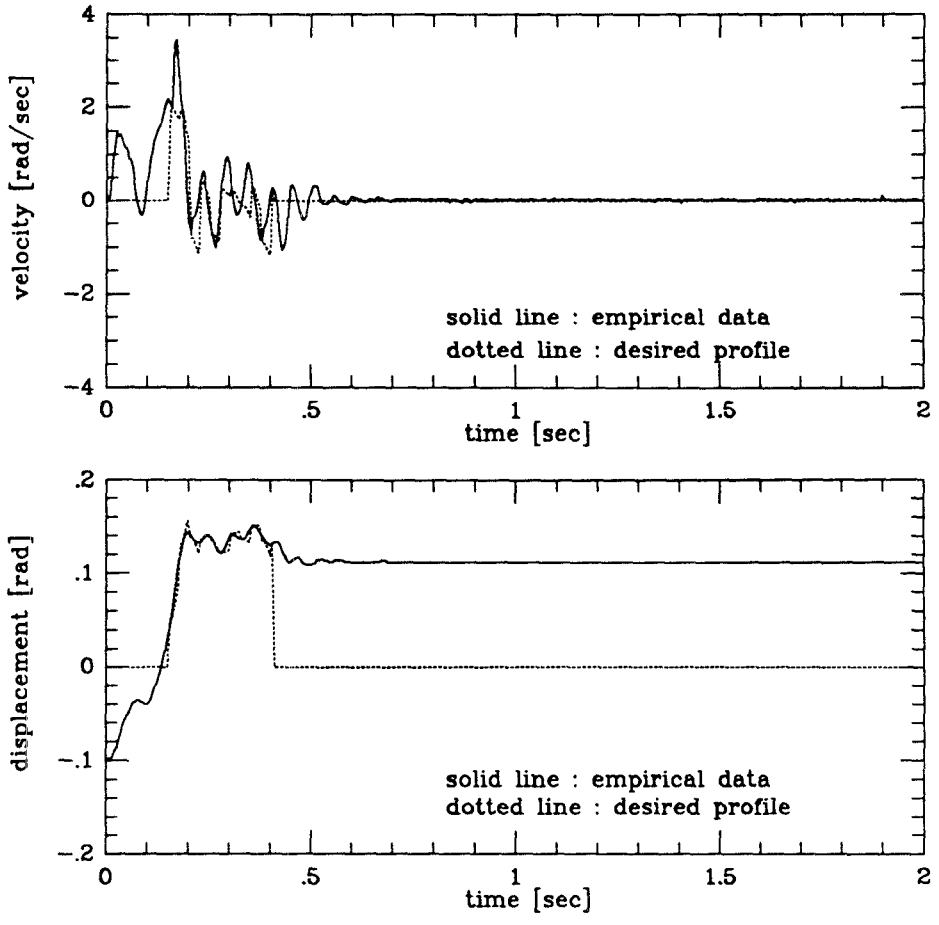

Figure 5.6: Position and velocity profiles for higher commanded force

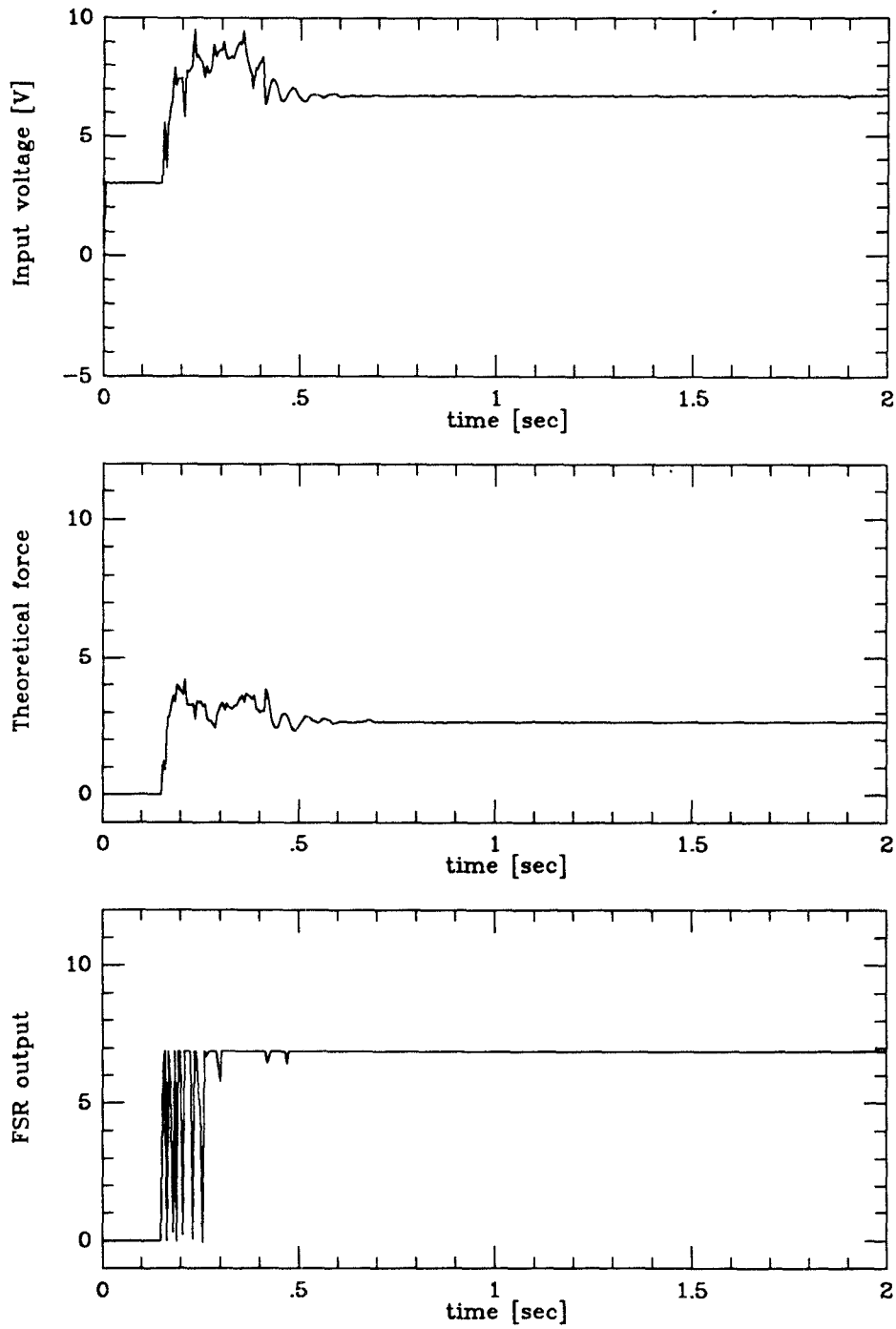

Figure 5.7: Force data and control signal to motor for higher commanded force

Chapter 6

Conclusions - suggestions for further research

Our work investigates the effect of impact that takes place when a flexible manipulator interacts with the environment. To summarize what has been presented here :

- We developed a finite element Galerkin model for the flexible manipulator in order to understand the impact behavior of the system. The model was validated through experimental results. The algebraic kinematic constraints that determine the constrained motion of the beam (together with the dynamic equations) were specified. The conventional numerical integration methods had to be slightly modified to accommodate impact-contact type problems. The simulation set-up can be conveniently used to investigate *off-line* new control schemes numerically.

- A detailed mathematical analysis of the phenomena that take place just before and just after contact (instantaneous velocity increments), led us to come up with a strategy for predicting the maximum impact force level in an amount of time suitable for real-time implementations. The corresponding method based on the energy principle was presented for the sake of comparison and its weaknesses were revealed.

- Finally, a newly proposed control strategy for reducing the effect of impact was demonstrated. *Our work treated the impact as a completely separate event by including the corresponding mode into the controller design.* Recall that previous designs attempted to diminish the impact force by tuning the force controller gains for the best transition response.

The current design is still in a quite primitive state since it does not exploit deeper analytical methods known for constraint problems. For example, the method that predicts the maximum reaction force can be extremely helpful in designing more refined position control laws for the free motion of the manipulator. These position control laws can give solutions to *minimal time* problems by not exceeding certain impending contact velocity thresholds, imposed by our method.

By providing the experimental set-up with additional state measurements, one can also lift the obvious limitations of the simplified model used in the inverse problem of the impact control scheme. Such additional measurements can

be: dependable force sensing (to be used in the steady-state[1]) and beam bending by installing piezo-films on the flexible arm. The latter can provide an estimate of the angle differences between the bodies modeling the beam. Improved performance can also be expected by increasing the sampling frequency and/or the available computing power.

Closing the discussion, we should state some important facts about the relation between impact and compliance. It is well known that all manipulators have some degree of inherent or deliberate compliance. This is very helpful, since in such a case the duration of impact is increased, granting the controller with more time to respond. However, it is to our advantage if deliberate compliance is present in a well-modeled way. Recall that accurate modeling is absolutely necessary in closed-loop endpoint force control, because it involves *noncollocated sensors and actuators.* Therefore, an experimental set-up where the arm consists of rigid bodies coupled with torsional springs of known stiffness is suggested for consideration. This kind of system surpasses the limitations of modeling a distributed parameter system and permits us to model the impact problem in a more direct and faithful way.

[1]It is worth noting that in our work we intentionally avoided explicit force feedback during the impact transient. This is advised for future designs as well, since almost all force transducers suffer from saturation during initial contact, although they may have exceptional rise times.

Appendix

List of C Source Code of the Numerical problem

```
/*************************************************************/
/* Program impact.c                                          */
/*                                                           */
/* This program predicts numerically the free, as well as the */
/* constrained motion of the flexible beam, using the Newmark */
/* approximation along with Newton-Raphson method for solving */
/* the non-linear system of dynamic equation that results.    */
/* It also predicts the maximum reaction force with two       */
/* different methods (by impact dynamics and by the energy    */
/* principle).                                               */
/* The time step of the Newmark approximation is 1 millisecond */
/* and the contact angle is 0.1 rad.                         */
/*************************************************************/

#include  <stdio.h>
#include  <math.h>
#include  "NumRecipesDouble/nr.h"
#include  "NumRecipesDouble/nrutil.h"
#include  "NumRecipesDouble/malloc.h"
#include  "defs.h"

double   *accel,*accel_0,*accel_1;
double   *vel_0,*vel_1,*disp_0,*disp_1;
double   dt,time,delay;
double   force,f_0,f_1,f_max;
double   input_voltage,load;
double   new_2,new_3;
int      nsteps,impact;
int      flag=0,count=0,pred_on=0;


main(argc,argv)
int argc;
char **argv;
{
int       s,r;
double    k,l;
```

```
double    sign();
double    predict_by_energy();
double    predict_by_dynamics();
double    reeval_accel();

       sscanf(argv[1],"%lf",&input_voltage);
       if (input_voltage<0.0 || input_voltage>10.0)
       {
          printf("\n invalid argument");
          exit(0);
       }

       s            = 0;
       dt           = STEP;
       nsteps       = NSTEPS;
       impact       = FALSE;
/**************Initialize vectors*******************************/
       accel_0 = dvector(1,3);
       accel_1 = dvector(1,3);
       accel   = dvector(1,3);
       vel_0   = dvector(1,3);
       vel_1   = dvector(1,3);
       disp_0  = dvector(1,3);
       disp_1  = dvector(1,3);
/**************Initial conditions*******************************/
       disp_0[1] = disp_0[2] = disp_0[3] = 0.0;
       vel_0[1]  = vel_0[2]  = vel_0[3]  = 0.0;
       accel_0[1]= accel_0[2]= accel_0[3]= 0.0;
       accel[1]  = accel[2]  = accel[3]  = 0.0;

       load = T*input_voltage;
/*************Start simulation*********************************/
       while(s<=nsteps)
       {
       time = s/1000.0;
       if(impact)
       {
          if(force>1e-6 || count==0)
          {
             flag = 1;
             Newmark(ITER);
             count++;
          }
```

```
          else if(force<=1e-6)   /* release condition */
          {
             flag = 0;
             Newmark(ITER);
             impact = FALSE;
             f_0 = f_1 = 0.0;
          }
       }
       else
       {
         f_0 = f_1 = 0.0;
         flag = 0;
         Newmark(ITER);
         count = 0;
       }
/************Update accelerations and velocities***************/
       for(r=1;r<=3;r++)
       {
         accel_1[r]=disp_1[r]-disp_0[r]-dt*vel_0[r]-dt*dt
                     *(0.5-BETA)*accel_0[r];
         accel_1[r] /= (dt*dt*BETA);

         vel_1[r] = vel_0[r]+dt*(1.0-GAMMA)*accel_0[r];
         vel_1[r] += dt*GAMMA*accel_1[r];
       }
/*************************************************************/
/* In the constrained motion  we should modify accelerations   */
/* and force, because of the instability of Newmark's method.  */
/* Velocities and displacements should be kept the same.       */
/* We proceed with the 4-dim system of equations as before,    */
/* for the same time step.                                     */
/*************************************************************/
       if (force>0.0 || count==1)
       {
         reeval_accel();
         if(force<0.0) force = 0.0;
/*************************************************************/
/* try to remove the above line to see that negative forces    */
/* result from  minor truncation errors and NOT from           */
/* instability.                                                */
/*************************************************************/
       }
       else{
```

```
        for(r=1;r<=3;r++) accel[r] = accel_1[r];
      }
/**************Check contact condition*************************/
      if(    !impact && count==0  && ((XI*sin(disp_1[3])-PSI*
                 cos(disp_1[3])-L*sin(disp_1[3]-disp_1[2]))>=0)
      {
         impact = TRUE;
         predict_by_energy();
         predict_by_dynamics();
         count  = 0;
      }
      else
      {
        for(r=1;r<=3;r++)
        {
          accel_0[r] = accel_1[r];
          disp_0[r]  = disp_1[r];
          vel_0[r]   = vel_1[r];
        }
        f_0 = f_1;
        printf(
        "%2.3f   %2.3f %2.3f   %2.3f %2.3f     %1.5f\n"
         ,time,disp_1[2],disp_1[3],vel_1[2],vel_1[3],force);
         s++;
      }
      }  /* end of ITER */
      free_vector(accel,1,3);
      free_vector(accel_0,1,3);
      free_vector(accel_1,1,3);
      free_vector(vel_0,1,3);
      free_vector(vel_1,1,3);
      free_vector(disp_0,1,3);
      free_vector(disp_1,1,3);
}  /*  End of main()  */


Newmark(iter)
int   iter;
{
  int m;
  double  tolx,tolf;
  double   **alpha,*bet,*x;
  void usrfun(),mnewt();
```

```
tolx=tolf= 1.0e-6;
if(!pred_on)
{
  if(!flag)                /* get free motion */
  {
    alpha =  dmatrix(1,3,1,3);
    bet   =  dvector(1,3);
    x     =  dvector(1,3);
    x[1] = disp_0[1];
    x[2] = disp_0[2];
    x[3] = disp_0[3];
    for(m=1;m<=iter;m++)
    {
    mnewt(1,x,3,tolx,tolf);
    usrfun(x,alpha,bet);
    }
    disp_1[1] = x[1];
    disp_1[2] = x[2];
    disp_1[3] = x[3];
    free_vector(x,1,3);
    free_vector(bet,1,3);
    free_matrix(alpha,1,3,1,3);
  }
  else                  /* get constrained motion */
  {
    alpha =  dmatrix(1,4,1,4);
    bet   =  dvector(1,4);
    x     =  dvector(1,4);
    x[1] = disp_0[1];
    x[2] = disp_0[2];
    x[3] = disp_0[3];
    x[4] = f_0;
    for(m=1;m<=iter;m++)
    {
    mnewt(1,x,4,tolx,tolf);
    usrfun(x,alpha,bet);
    }
    disp_1[1] = x[1];
    disp_1[2] = x[2];
    disp_1[3] = x[3];
    f_1 = x[4];
    free_vector(x,1,4);
```

```
      free_vector(bet,1,4);
      free_matrix(alpha,1,4,1,4);
    }
  }
  else    /* i.e. prediction is on */
  {
    alpha =  dmatrix(1,3,1,3);
    bet   =  dvector(1,3);
    x     =  dvector(1,3);
    x[1] = 5.0;
    x[2] = 5.0;
    x[3] = 1.0;   /* initial guess for input voltage 1V  */
    for(m=1;m<=(iter*3);m++)
    {
    mnewt(1,x,3,tolx,tolf);
    usrfun(x,alpha,bet);
    }
    delay = x[1];
    f_max = x[2];
    pred_on = FALSE;
    free_vector(x,1,3);
    free_vector(bet,1,3);
    free_matrix(alpha,1,3,1,3);
  }
}


void  usrfun(x,alpha,bet)
/*****************************************************************/
/* this routine determines the Jacobians of the non-linear     */
/* system of equations that results from the Newmark           */
/* approximation                                               */
/*****************************************************************/
double   **alpha,*bet,*x;
{
int        i;
double     *a,*v;
double     sign();
double     dif_1,dif_2;

  if(!pred_on)
  {
    a   =  dvector(1,3);
```

```
    v   =  dvector(1,3);
/*******************Predictors*********************************/
    for(i=1;i<=3;i++){
      a[i]=x[i]-disp_0[i]-dt*vel_0[i]-dt*dt*(.5-BETA)*accel_0[i];
      a[i]/=(dt*dt*BETA);

      v[i] = vel_0[i]+dt*((1.0-GAMMA)*accel_0[i]+GAMMA*a[i]);
    }
/*****************Jacobian*************************************/
    if(!flag)
    {
      alpha[1][1] =I1/(dt*dt*BETA)+K1+(KT*KB/RA)*GAMMA/(dt*BETA);
      alpha[1][1] += K_FRICT*GAMMA/(dt*BETA);
      alpha[1][2] =-K1;
      alpha[1][3] =0.0;
      alpha[2][1] =-K1;
      alpha[2][2] =K1+K2+(M2*E2*E2+M3*L*L+I2+M3*L*E3
                  *cos(x[3]-x[2])) /(dt*dt*BETA);
      alpha[2][2] +=a[2]*M3*L*E3*sin(x[3]-x[2]);
      alpha[2][2] +=a[3]*M3*L*E3*sin(x[3]-x[2]);
      alpha[2][2] +=M3*L*E3*cos(x[3]-x[2])*(v[3]*v[3]-v[2]*v[2]);
      alpha[2][2] +=M3*L*E3*sin(x[3]-x[2])*2.0*v[2]*GAMMA
                          /(dt*BETA);
      alpha[2][3] =-K2-a[2]*M3*L*E3*sin(x[3]-x[2]);
      alpha[2][3] +=(M3*E3*E3+I3+M3*L*E3*cos(x[3]-x[2]))
                         /(dt*dt*BETA);
      alpha[2][3] -=a[3]*M3*L*E3*sin(x[3]-x[2]);
      alpha[2][3] -=M3*L*E3*cos(x[3]-x[2])*(v[3]*v[3]-v[2]*v[2]);
      alpha[2][3] -=M3*L*E3*sin(x[3]-x[2])*2.0*v[3]*GAMMA
                         /(dt*BETA);
      alpha[3][1] =0.0;
      alpha[3][2] =-K2+M3*L*E3*cos(x[3]-x[2])/(dt*dt*BETA);
      alpha[3][2] +=M3*L*E3*sin(x[3]-x[2])*a[2];
      alpha[3][2] +=M3*L*E3*sin(x[3]-x[2])*2.0*v[2]*GAMMA
                          /(dt*BETA);
      alpha[3][2] -=M3*L*E3*cos(x[3]-x[2])*v[2]*v[2];
      alpha[3][3] =K2-M3*L*E3*sin(x[3]-x[2])*a[2];
      alpha[3][3] +=(M3*E3*E3+I3)/(dt*dt*BETA)
                       +M3*L*E3*cos(x[3]-x[2])*v[2]*v[2];
      bet[1] =I1*a[1]+K1*x[1]-K1*x[2]+K_FRICT*(v[1])
               -load+(KT*KB/RA)*v[1]+STICTION*sign(v[1]);
      bet[2] =K2*(x[2]-x[3])+K1*(x[2]-x[1]);
      bet[2] +=(M2*E2*E2+M3*L*L+I2+M3*L*E3*cos(x[3]-x[2]))*a[2];
```

```
  bet[2] +=(M3*E3*E3+I3+M3*L*E3*cos(x[3]-x[2]))*a[3];
  bet[2] -=M3*L*E3*(sin(x[3]-x[2]))*(v[3]*v[3]-v[2]*v[2]);
  bet[3] =K2*(x[3]-x[2])+M3*L*E3*(cos(x[3]-x[2]))*a[2];
  bet[3] +=(M3*E3*E3+I3)*a[3]
                +M3*L*E3*sin(x[3]-x[2])*v[2]*v[2];
  for(i=1;i<=3;i++) bet[i] *= -1.0;
}
else
{
  alpha[1][1] =I1/(dt*dt*BETA)+K1+(KT*KB/RA)*GAMMA/(dt*BETA);
  alpha[1][1] +=K_FRICT*GAMMA/(dt*BETA);
  alpha[1][2] =-K1;
  alpha[1][3] =0.0;
  alpha[1][4] =0.0;
  alpha[2][1] =-K1;
  alpha[2][2] =K1+K2+(M2*E2*E2+M3*L*L+I2+M3*L*E3
                  *cos(x[3]-x[2])) /(dt*dt*BETA);
  alpha[2][2] +=a[2]*M3*L*E3*sin(x[3]-x[2]);
  alpha[2][2] +=a[3]*M3*L*E3*sin(x[3]-x[2]);
  alpha[2][2] +=M3*L*E3*cos(x[3]-x[2])*(v[3]*v[3]-v[2]*v[2]);
  alpha[2][2] +=M3*L*E3*sin(x[3]-x[2])*2.0*v[2]*GAMMA
                   /(dt*BETA);
  alpha[2][2] +=x[4]*L*sin(x[3]-x[2]);
  alpha[2][3] =-K2-a[2]*M3*L*E3*sin(x[3]-x[2]);
  alpha[2][3] +=(M3*E3*E3+I3+M3*L*E3*cos(x[3]-x[2]))
                   /(dt*dt*BETA);
  alpha[2][3] -=a[3]*M3*L*E3*sin(x[3]-x[2]);
  alpha[2][3] -=M3*L*E3*cos(x[3]-x[2])*(v[3]*v[3]-v[2]*v[2]);
  alpha[2][3] -=M3*L*E3*sin(x[3]-x[2])*2.0*v[3]*GAMMA
                     /(dt*BETA);
  alpha[2][3] -=x[4]*L*sin(x[3]-x[2]);
  alpha[2][4] =L*(1.0+cos(x[3]-x[2]));
  alpha[3][1] =0.0;
  alpha[3][2] =-K2+M3*L*E3*cos(x[3]-x[2])/(dt*dt*BETA);
  alpha[3][2] +=M3*L*E3*sin(x[3]-x[2])*a[2];
  alpha[3][2] +=M3*L*E3*sin(x[3]-x[2])*2.0*v[2]*GAMMA
                   /(dt*BETA);
  alpha[3][2] -=M3*L*E3*cos(x[3]-x[2])*v[2]*v[2];
  alpha[3][3] =K2-M3*L*E3*sin(x[3]-x[2])*a[2];
  alpha[3][3] +=(M3*E3*E3+I3)/(dt*dt*BETA)
                 +M3*L*E3*cos(x[3]-x[2])*v[2]*v[2];
  alpha[3][4] =L;
  alpha[4][1] =0.0;
```

```
    alpha[4][2] =L*cos(x[3]-x[2]);
    alpha[4][3] =XI*cos(x[3])+PSI*sin(x[3])-L*cos(x[3]-x[2]);
    alpha[4][4] =0.0;
    bet[1] =I1*a[1]+K1*x[1]-K1*x[2]+K_FRICT*(v[1])
              -load+(KT*KB/RA)*v[1] +STICTION*sign(v[1]);
    bet[2] =K2*(x[2]-x[3])+K1*(x[2]-x[1]);
    bet[2] +=(M2*E2*E2+M3*L*L+I2+M3*L*E3*cos(x[3]-x[2]))*a[2];
    bet[2] +=(M3*E3*E3+I3+M3*L*E3*cos(x[3]-x[2]))*a[3];
    bet[2] -=M3*L*E3*(sin(x[3]-x[2]))*(v[3]*v[3]-v[2]*v[2]);
    bet[2] +=x[4]*L*(1.0+cos(x[3]-x[2]));
    bet[3] =K2*(x[3]-x[2])+M3*L*E3*(cos(x[3]-x[2]))*a[2];
    bet[3] +=(M3*E3*E3+I3)*a[3]+M3*L*E3*sin(x[3]-x[2])
               *v[2]*v[2];
    bet[3] +=x[4]*L;
    bet[4] =XI*sin(x[3])-PSI*cos(x[3])-L*sin(x[3]-x[2]);
    for(i=1;i<=4;i++) bet[i] *= -1.0;
  }
}
else      /*  i.e. prediction is on */
{
  dif_2 = disp_0[3]-disp_0[2];
  dif_1 = disp_0[2]-disp_0[1];

  alpha[1][1] =-load -K1*dif_1-K1*x[1]*(new_2-x[3])/2.0+
                    ((KT*KB/RA)+K_FRICT)*x[3]/2.0+STICTION;
  alpha[1][2] =0.0;
  alpha[1][3] =-I1+K1*x[1]*x[1]/4.0+((KT*KB/RA)
                      +K_FRICT)*x[1]/2.0;
  alpha[2][1] =-K2*dif_2-K2*x[1]*(new_3-new_2)/2.0+K1*dif_1+
   K1*x[1]*(new_2-x[3])/2.0+(1.0+cos(dif_2))*x[2]/4.0;
  alpha[2][2] =(1.0+cos(dif_2))*x[1]/4.0;
  alpha[2][3] =-K1*x[1]*x[1]/4.0;
  alpha[3][1] =K2*dif_2+K2*x[1]*(new_3-new_2)/2.0
                     +x[2]/4.0;
  alpha[3][2] =x[1]/4.0;
  alpha[3][3] =0.0;
  bet[1] =-I1*x[3]-K1*x[1]*dif_1-K1*x[1]*x[1]*(new_2-x[3])/4.0
  -load*x[1]+((KT*KB/RA)+K_FRICT)*x[1]*x[3]/2.0+STICTION*x[1];
  bet[2] =-K2*x[1]*dif_2-K2*x[1]*x[1]*(new_3-new_2)/4.0;
  bet[2] +=K1*x[1]*dif_1+K1*x[1]*x[1]*(new_2-x[3])/4.0;
  bet[2] +=-7.0*M2*E2*E2*new_2-3.0*M2*E2*E2*new_3+
                 (1.0+cos(dif_2))*x[1]*x[2]/4.0;
  bet[3] =K2*x[1]*dif_2+K2*x[1]*x[1]*(new_3-new_2)/4.0;
```

```
    bet[3] +=-2.0*M2*E2*E2*cos(dif_2)*new_2-(M2*E2*E2+I3)*new_3
                  +x[1]*x[2]/4.0;
    for(i=1;i<=3;i++) bet[i] *= -1.0;
  }
}


double sign(number)
double number;
{
  double s;
  if(number<=1.0e-5 && number>=-1.0e-2) s = 0.0;
  if(number>1.0e-5) s = 1.0;
  if(number<-1.0e-5) s = -1.0;
  return(s);
}


double predict_by_energy()
/*****************************************************************/
/* this routine predicts the maximum reaction force at the tip */
/* using the energy principle                                  */
/*****************************************************************/
{
double kinetic;
double cosine;
double angle_dif,d2_max,d3_max;
double f_impact;
double   **a;
double   **b;      /* ax=b  */

        a  = dmatrix(1,3,1,3);
        b  = dmatrix(1,3,1,3);
        cosine = cos(disp_0[3]-disp_0[2]);
        kinetic =0.5*I1*vel_0[1]*vel_0[1];
        kinetic +=0.5*M2*E2*E2*vel_0[2]*vel_0[2];
        kinetic +=0.5*M3*(L*L*vel_0[2]*vel_0[2]
         +E2*E2*vel_0[3]*vel_0[3]+E2*vel_0[2]*vel_0[3]*cosine);
        kinetic +=0.5*K2*(disp_0[3]-disp_0[2])
                        *(disp_0[3]-disp_0[2]);
            /* the potential portion is also included above */
        angle_dif =sqrt(2.0*kinetic/K2);
        d2_max =0.1+angle_dif/2.0;
```

```
        d3_max =0.1-angle_dif/2.0;

        a[1][1] = M2*E2*E2+M3*L*L+I2+M3*L*E3*cos(angle_dif);
        a[1][2] = M3*E3*E3+I3+M3*L*E3*cos(angle_dif);
        a[1][3] = L*(1.0+cos(angle_dif));
        a[2][1] = M3*L*E3*cos(angle_dif);
        a[2][2] = M3*E3*E3+I3;
        a[2][3] = L;
        a[3][1] = L*cos(angle_dif);
        a[3][2] = L;
        a[3][3] = 0.0;
        b[1][1] = -K2*angle_dif+load;
        b[2][1] = K2*angle_dif;
        b[3][1] = 0.0;

        gaussj(a,3,b,3);

        f_impact = b[3][1];

        printf("for K2=%f and input=%1.1f\n",K2,input_voltage);
        printf("prediction by energy: %1.4f \n",f_impact);
        free_matrix(a,1,3,1,3);
        free_matrix(b,1,3,1,3);
}


double predict_by_dynamics()
/*****************************************************************/
/* this routine predicts the maximum reaction force at the tip */
/* using the impact dynamics                                    */
/*****************************************************************/
{
double cosine;
double a,b,c,d,e,f,u;
double del2,del3;

        cosine = cos(disp_0[3]-disp_0[2]);
        u = -(L*cosine*vel_0[2]+(XI*cos(disp_0[3])
             +PSI*sin(disp_0[3])-L*cosine)*vel_0[3]);
        a = 7.0*M2*E2*E2;
        b = 3.0*M2*E2*E2;
        c = 2.0*M2*E2*E2*cosine;
        d = M2*E2*E2+I3;
```

```
        e = (d*(1.0+cosine)-b)*(-L)/(a*d-b*c);
        f = (-c*(1.0+cosine)+a)*(-L)/(a*d-b*c);
        f_imp=u/(L*cosine*e+(XI*cos(disp_0[3])
              +PSI*sin(disp_0[3])-L*cosine)*f);
        del2 = f_imp*e;
        del3 = f_imp*f;
        new_2 = vel_0[2]+del2;
        new_3 = vel_0[3]+del3;

        printf("new 2 : %f \n",new_2);
        printf("new 3 : %f \n",new_3);

        pred_on = TRUE;
        Newmark(ITER);
        printf("prediction by dynamics  : %1.4f \n",f_max);
        printf("delay    : %1.4f \n",delay);
}


double reeval_accel()
{
double cosine;
double   **a;
double   **b;      /* ax=b  */
        a  = dmatrix(1,3,1,3);
        b  = dmatrix(1,3,1,3);
/************the 4 unknowns are force,accel[i]*****************/
        cosine = cos(disp_1[3]-disp_1[2]);
        accel[1]=load+K1*(disp_1[2]-disp_1[1]) -K_FRICT*vel_1[1];
        accel[1]+=-(KT*KB/RA)*vel_1[1]-STICTION*sign(vel_1[1]);
        accel[1]/=I1;
        a[1][1]=M2*E2*E2+M3*L*L+I2+M3*L*E3*cosine;
        a[1][2]=M3*E3*E3+I3+M3*L*E3*cosine;
        a[1][3]=L*(1.0+cosine);
        b[1][1]=K2*(disp_1[3]-disp_1[2])
                     -K1*(disp_1[2]-disp_1[1]);
        b[1][1]+=M3*L*E3*sin(disp_1[3]-disp_1[2])
                 *(vel_1[3]*vel_1[3] -vel_1[2]*vel_1[2]);
        a[2][1]=M3*L*E3*cosine;
        a[2][2]=M3*E3*E3+I3;
        a[2][3]=L;
        b[2][1]=-K2*(disp_1[3]-disp_1[2]);
        b[2][1]+=-M3*L*E3*sin(disp_1[3]-disp_1[2])
```

```
                    *vel_1[2]*vel_1[2];
        a[3][1]=L*cosine;
        a[3][2]=XI*cos(disp_1[3])+PSI*sin(disp_1[3])-L*cosine;
        a[3][3]=2.0*L*sin(disp_1[3]-disp_1[2])*vel_1[2]*vel_1[3];
        b[3][1]+=-L*sin(disp_1[3]-disp_1[2])*vel_1[2]*vel_1[2];
        b[3][1]+=-(-XI*sin(disp_1[3])+PSI*cos(disp_1[3])
                  +L*sin(disp_1[3]-disp_1[2]))*vel_1[3]*vel_1[3];

        gaussj(a,3,b,3);

        accel[2] = b[1][1];
        accel[3] = b[2][1];
        force    = b[3][1];
        free_matrix(a,1,3,1,3);
        free_matrix(b,1,3,1,3);
}
```

Bibliography

[1] J. D. Bartusek. Design and digital signal processor implementation of a controller for flexible structures. Master's thesis, University of Maryland, College Park, 1989.

[2] Bayo E. A finite element approach to control the end point motion of a single link flexible robot. *Journal of Robotic Systems*, 4(1), 1987.

[3] Bayo E. and Paden B. On trajectory generation of flexible robots. *Journal of Robotic Systems*, 4(2), 1987.

[4] G.H. Frank. Design and real-time control of a flexible arm. Master's thesis, University of Maryland, College Park, 1986.

[5] Chae H. and John M. Hollerbach. Dynamic stability issues in force control of manipulators. *IEEE Robotics and Automation Conference*, pages 890–896, 1987.

[6] T.J.R. Hughes. *The Finite Element Method.* Prentice-Hall, 1987.

[7] F.M.L. Amirouche J. Kahng. Impact force analysis in mechanical hand design. *IEEE J. of Robotics and Automation*, 1987.

[8] Mills J.K. Manipulator transition to and from contact tasks: A discontinuous control approach. *Proc. IEEE Int. Conf. on Robotics and Automation*, May 1990a.

[9] Mills J.K. A generalized lyapunov approach to robotic manipulator stability during transition to and form contact tasks. *Proc. Japan-U.S.A. Symposium on Flexible Automation, Kyoto, Japan*, July 9-13 1990c.

[10] Mills J.K. and Goldenberg A.A. Force and position control of manipulators during constrained motion tasks. *IEEE J. of Robotics and Automation*, 5(1), 1989.

[11] Mills J.K. and Lokhorst D.M. Experimental results in manipulator contact task control. *IEEE Int. Conf. on Robotics and Automation, Sacramento, California*, April 1991.

[12] L. Meirovitch. *Analytical Methods in Vibrations.* Macmillan, New York, 1969.

[13] L. Meirovitch. *Dynamics and Control of Structures.* J. Wiley, 1990.

[14] Spong M.W. and Vidyasagar M. *Robot Dynamics and Control.* John Wiley, 1988.

[15] N.M. Newmark. A method of computation for structural dynamics. *Journal of the Engineering Mechanics Division, ASCE*, pages 67–94, 1959.

[16] T. Parker and F. Paul. Impact force control in robot hand design. *ASME Proc., Winter Annual Meeting*, December 1985.

[17] T. A. Posbergh. *Modeling and Control of Mixed and Flexible Structures.* PhD thesis, University of Maryland, College Park, 1988.

[18] Johnson R.C. *Impact Forces in mechanisms.* Machine Design, June 12 1958.

[19] Eppinger S. and W. Seering. On dynamic models of robot force control. *Proc. of the International Conf. on Robotics and Automation, IEEE*, March 1986.

[20] Eppinger S. and W. Seering. Understanding bandwidth limitations in robot force control. *Proc. of the International Conf. on Robotics and Automation, IEEE*, April 1987.

[21] W. Press B. Flannery S. Teukolsky W. Vetterling. *Numerical Recipes in C.* Cambridge, 1988.

[22] R. Volpe and P. Khosla. Experimental verification of a stategy for impact control. *IEEE Int. Conf. on Robotics and Automation, Sacramento, California*, April 1991.

[23] L.S. Wang. Control system design for a flexible arm. Master's thesis, University of Maryland, College Park, 1987.

[24] Y. Wang and M.T. Mason. Modeling impact dynamics for robotic operations. *IEEE Int. Conf. on Robotics and Automation, Raleigh, NC*, pages 678–685, 1986.

[25] D. Whitney. Historical perspective and state of the art in robot force control. *IEEE Int. Conf. on Robotics and Automation*, March 1985.

[26] J. Wittenburg. *Dynamics of Systems of Rigid Bodies.* B. G. Teubner Stuttgart, 1977.

[27] Youcef-Toumi, K., and Gutz D. Impact and force control. *IEEE Int. Conf. on Robotics and Automation*, pages 410–416, April 1989.

[28] K. Youcef-Toumi and D. Li. Force control of direct drive manipulators for surface following. *IEEE Int. Conf. on Robotics and Automation, Sacramento, California*, April 1987.